THE RESPONSE OF ACCRETION DISKS TO BENDING WAVES: ANGULAR MOMENTUM TRANSPORT AND RESONANCES

CAROLINE E.J.M.L.J. TERQUEM¹

UCO/Lick Observatory, University of California, Santa Cruz, CA 95064; Isaac Newton Institute for Mathematical Sciences, University of Cambridge, 20 Clarkson Road, Cambridge, CB3 0EH, UK; ct@ucolick.org

The Astrophysical Journal, 509:000-000, 1998 December 20

ABSTRACT

We investigate the linear tidal perturbation of a viscous Keplerian disk by a companion star orbiting in a plane inclined to the disk. We consider m=1 perturbations with odd symmetry with respect to the z=0 midplane. The response frequency may be either finite or vanishing. These long-wavelength perturbations produce a well-defined warp.

Since the response of a viscous disk is not in phase with the perturbing potential, a tidal torque is exerted on the disk. When the perturber rotates outside the disk, this torque results in a decrease of the disk angular momentum, and thus in an increase of its accretion rate.

We show that this tidal torque is comparable to the horizontal viscous stress acting on the background flow when the perturbed velocities in the disk are on the order of the sound speed. If these velocities remain subsonic, the tidal torque can exceed the horizontal viscous stress only if the viscous parameter $\alpha_{\rm v}$ which couples to the vertical shear is larger than the parameter $\alpha_{\rm h}$ coupled to the horizontal shear. In protostellar disks, bending waves, which are predominantly excited in the outer regions, are found to propagate and transport a significant fraction of the negative angular momentum they carry deep into the disk inner parts.

If the waves are reflected at the center, resonances occur when the frequency of the tidal waves is equal to that of some free normal global bending mode of the disk. If such resonances exist, tidal interactions may then be important even when the binary separation is large. Out of resonance, the torque associated with the secular perturbation, which is proportional to $\alpha_{\rm v}$, is generally much larger than that associated with the finite frequency perturbations. As long as the waves are damped before they reach the center, the torque associated with the finite frequency perturbations does not depend on the viscosity, in agreement with theoretical expectation. These calculations are relevant to disks around young stars and maybe also to disks in X–ray binary systems.

Subject headings: accretion, accretion disks — binaries: general — hydrodynamics — stars: pre-main sequence — waves

1. INTRODUCTION

1.1. Tidal Interactions in Pre-main-Sequence Binary Systems: Coplanar versus Noncoplanar Systems

Thanks to recent optical images taken with the *Hubble Space Telescope*, accretion disks around low-mass pre-main sequence stars known as T Tauri are no longer objects of theoretical speculations (McCaughrean & O'Dell 1996). As expected, they appear to be common around young stars (Stauffer et al. 1994). Furthermore, most T Tauri stars are observed to be in multiple systems (see Mathieu 1994 and references therein). Since the distribution of the separation of pre-main sequence binaries has a peak around 30 astronomical units, which is smaller than the extent of the disks in such systems (Edwards et al. 1987), it is expected that many circumstellar disks will be subject to tidal effects due to the influence of binary companions.

The theory of tidal interaction has already successfully satisfied many observational tests. For example, it has been predicted that angular momentum exchange between orbital motion and disk rotation through tidal interaction may truncate the disk (see, e.g., Papaloizou &

Pringle 1977; Paczyński 1977). This has recently received observational confirmation, both through the study of young binaries spectra (Dutrey, Guilloteau & Simon 1994; Jensen, Mathieu & Fuller 1996) and direct imaging (Roddier et al. 1996).

The tidal effect of an orbiting body on a differentially rotating disk has been well studied in the context of planetary rings (Goldreich & Tremaine 1978), planet formation, and interacting binary stars (see Lin & Papaloizou 1993 and references therein). In these studies, the disk and orbit are usually taken to be coplanar. However, there are observational indications that the plane of the disk and that of the orbit may not necessarily be aligned. The most striking evidence for such noncoplanarity is given by HST and adaptive optics images of the pre-main sequence binary HK Tau (Stapelfeldt et al. 1998). The projected binary separation in this system is 340 AU, the observed radius of the circumsecondary disk is 105 AU and the disk aspect ratio at a radius of 50 AU is about 0.08. The authors suggest that the primary would be located at an angle of at least 20° above the disk plane. In the case of the hierarchical triple system Ty Cra, some models suggest that the orbit of the close spectroscopic binary and that of the

¹On leave from Laboratoire d'Astrophysique, Observatoire de Grenoble, Université Joseph Fourier/CNRS, 38041 Grenoble Cedex 9, France

wider binary are not in the same plane (see Corporon, Lagrange & Beust 1996; Bibo, The & Dawanas 1992). Also, observations of the pre-main sequence binary T Tau have revealed that two bipolar outflows of very different orientations originate from this system (Böhm & Solf 1994). Since it is unlikely that they are both ejected by the same star, each of them is more probably associated with a different member of the binary. Furthermore, jets are usually thought to be ejected perpendicularly to the disk from which they originate. These observations then suggest that disks and orbit are not coplanar in this binary system. More generally, observations of molecular outflows in star forming regions commonly show several jets of different orientations emanating from unresolved regions of extent as small as a few hundred astronomical units (Davis, Mundt & Eislöffel 1994).

We note that the spectral energy distribution of a circumstellar disk could be significantly affected by the lack of coplanarity in binary or multiple systems (Terquem & Bertout 1993, 1996). This is because reprocessing of radiation from the central star by a disk depends crucially on the disk geometry.

In such noncoplanar systems, both density and bending waves are excited in the disk by the perturbing companion. They are respectively of even and odd symmetry with respect to reflection in the disk mid-plane. Since much work has already been carried out on density waves, which are the only waves excited in coplanar systems, we shall focus here on bending waves. Because their wavelength is larger than that of density waves, they are expected to propagate and transport angular momentum further radially into the disk.

1.2. Bending Waves

Bending waves were first studied by Hunter & Toomre (1969) in the context of the Galactic disk. They calculated the dispersion relation associated with these waves taking into account self-gravity but ignoring pressure and viscosity. Bending waves were further considered in the context of galactic disks (Toomre 1983; Sparke 1984; Sparke & Casertano 1988) and planetary rings (Shu, Cuzzi & Lissauer 1983; Shu 1984). In these studies, the horizontal motions associated with the vertical displacement of the disk were neglected. However, Papaloizou & Pringle (1983) showed that these motions are important in gaseous Keplerian disks, where they are nearly resonant. These authors pointed out that when the disk is sufficiently viscous so that its response to vertical displacements is diffusive rather than wave-like, these motions lead to the decay timescale of the warp being $\alpha_{\rm v}^2$ times the viscous timescale $t_{\nu,v}$. Here α_v is the Shakura & Sunyaev (1973) parameter that couples to the vertical shear, and $t_{\nu,\nu}$ is the disk viscous timescale associated to $\alpha_{\rm v}$. When $\alpha_{\rm v}$ is smaller than unity, this timescale is smaller than $t_{\nu,\nu}$, which is the decay timescale of the warp obtained by previous authors.

In the context of protostellar disks, Artymowicz (1994) studied the orbital evolution of low–mass bodies crossing disks, and Ostriker (1994) calculated the angular momentum exchange between an inviscid disk and a perturber on a near–parabolic noncoplanar orbit outside the disk (see also Heller 1995 for numerical simulations). The vertical

structure of the disk was not taken into account in these studies. Papaloizou & Lin (1995) performed a full 3 dimensional linear analysis of m=1 bending waves in accretion disks. Comparing analytical results with numerical simulations, they showed that a vertical averaging approximation can be used when the wavelength of the perturbation is much larger than the disk semi-thickness. Using the WKB approximation, they calculated the dispersion relation associated with bending waves taking into account self-gravity, pressure and viscosity (see also Masset & Tagger 1996 for a study of thick disks). They found that in a non self-gravitating thin Keplerian disk in which $\alpha_{\rm v}$ is small compared to the disk aspect ratio, bending waves propagate without dispersion at a speed which is about half the sound speed. Using these results, Papaloizou & Terquem (1995) calculated the m=1 bending wave response of an inviscid disk with the rotation axis misaligned with a binary companion's orbital rotation axis. work was extended by Larwood et al. (1996) who performed nonlinear calculations of the disk response using smoothed particle hydrodynamics (SPH). This numerical method was further used by Larwood & Papaloizou (1997) who analyzed the response of a circumbinary disk subject to the tidal forcing of a binary with a fixed noncoplanar circular orbit, and by Larwood (1997) who considered the tidal interaction occurring between a disk and a perturber following a parabolic trajectory inclined with respect to the disk.

The present work should be contrasted with earlier studies of purely viscous disks in which pressure and self-gravity were ignored. The behavior of nonplanar purely viscous accretion disk subject to external torques has been considered previously by a number of authors. Following the analysis of Bardeen & Petterson (1975), these studies have been developed in connection with the precessing disks of Her X-1 and SS 433 for instance (e.g., Petterson 1977; Katz 1980a, 1980b), galactic warps (e.g., Steiman–Cameron & Durisen 1988), or warped disks around AGN and in X-ray binaries (Pringle 1996). However, the response of a purely viscous disk is very different from that of a viscous gaseous disk, which is a better representation of a protostellar disk. In the former case, evolution occurs only through viscous diffusion, whereas in the latter case pressure effects manifesting themselves through bending waves can control the disk evolution. When these waves propagate (i.e. when they are not damped), they do so on a timescale comparable to the sound crossing time. Since this is much shorter than the viscous diffusion timescale, communication through the disk occurs as a result of the propagation of these waves. Even when the waves are damped before reaching the disk boundary, a diffusion coefficient for warps that is much larger than that produced by the kinematic viscosity may occur because of pressure effects (Papaloizou & Pringle 1983). Self-gravity may also strongly modify the response of viscous disks, because like pressure it allows bending waves to propagate and its effect is global. For a more detailed discussion of the respective effects of viscosity, pressure and self-gravity, see Papaloizou, Terquem & Lin (1998).

1.3. Torque Exerted on the Disk by a Companion on an Inclined Orbit There can be no tidal torque exerted on an inviscid disk with reflective boundaries that contains no corotation resonance (Goldreich & Nicholson 1989). However, if the disk is viscous or has a nonreflective boundary, the companion exerts a torque on the disk that leads to an exchange of angular momentum between the disk rotation and the orbital motion. We can distinguish the following three components of the torque:

- 1. The component along the line of nodes makes the disk precess at a rate that can be uniform (see § 5.2 and Kuijken 1991; Papaloizou & Terquem 1995; Papaloizou et al. 1998). Although we will calculate in this paper the precession frequency induced by the tidal torque, we will not discuss the disk precession in detail since this has already been done in the papers cited above.
- 2. The component of the torque along the axis perpendicular to the line of nodes in the disk plane induces the evolution of the inclination angle of the disk plane with respect to that of the orbit. This evolution, which is not necessarily toward coplanarity, occurs on the disk's viscous timescale if the warp is linear (Papaloizou & Terquem 1995; Papaloizou et al. 1998). Since it affects the geometry of the system only on such a long timescale, we will not discuss this effect here. We note that both these components of the tidal torque modify the direction of the disk angular momentum vector.
- 3. The component of the torque along the disk's spin axis does not modify the direction but the modulus of the disk's angular momentum vector, thus changing the disk's accretion rate. This effect is important since it is a source of angular momentum transport in the disk, and it will be the main subject of this paper.

So far, angular momentum exchange between a viscous gaseous disk rotation and the orbital motion of a companion on an inclined circular orbit has not been considered. It is the goal of this paper to present an analysis of this process. In the case of an inviscid disk considered by Papaloizou & Terquem (1995), such angular momentum exchange occurs because the waves are assumed to interact nonlinearly with the background flow before reaching the disk's inner boundary. Thus, only in-going waves propagate through the disk. This induces a lag between the disk response and the perturbation, which enables a torque to be exerted on the disk. In a viscous disk, the lag required for the torque to be non zero is naturally produced by the viscous shear stress.

1.4. Plan of the Paper

The plan of the paper is as follows. In \S 2 we derive an expression for the perturbing potential. In \S 3 we outline the basic equations. The model of the unperturbed disk is described in \S 4. The disk response is presented in \S 5, where we give the linearized equations, study the disk response for both zero and finite perturbing frequencies, establish the boundary conditions and describe the domain of validity of this analysis. In \S 6 we calculate the torque exerted by the perturber on the disk, and relate it to the disk viscosity by using the conservation of angular momentum. We show that this tidal torque is comparable to the horizontal viscous stress acting on the background flow when the perturbed velocities in the disk are on the order of the sound speed. If these velocities remain subsonic, the

tidal torque can exceed the horizontal viscous stress only if the viscous parameter $\alpha_{\rm v}$ that couples to the vertical shear is larger than the parameter α_h coupled to the horizontal shear. Numerical results are presented in § 7, both for uniform and nonuniform viscosity. They indicate that, for parameters typical of protostellar disks, bending waves are able to propagate and transport a significant fraction of the negative angular momentum they carry deep into the inner parts of the disk. They also show that, if the waves can be reflected at the disk's inner boundary, resonances occur when the frequency of the tidal waves is equal to that of some free normal global bending mode of the disk. Out of resonance, if the disk and the orbital planes are not too close to being perpendicular, the torque associated with the zero-frequency perturbing term is found to be much larger than that associated with the finite frequency terms. As long as the waves are damped before they reach the center, the torque associated with the finite frequency perturbations does not depend on the viscosity, in agreement with theoretical expectation (Goldreich & Tremaine 1982). We summarize and discuss our results in \S 8.

2. PERTURBING POTENTIAL

We consider a binary system in which the primary has a mass M_p and the secondary has a mass M_s . The binary orbit is circular with separation D. We suppose that the primary is surrounded by a disk of radius $R \ll D$ and of negligible mass M so that the orbital plane does not precess and the secondary describes a prograde Keplerian orbit with angular velocity:

$$\omega = \sqrt{\frac{G\left(M_s + M_p\right)}{D^3}},$$

about the primary. In the absence of the secondary star, the disk is nearly Keplerian. We adopt a nonrotating Cartesian coordinate system (x,y,z) centered on the primary star. The z-axis is chosen to be normal to the initial disk mid-plane. We shall also use the associated cylindrical polar coordinates (r,φ,z) . The orbit of the secondary star is in a plane that has an initial inclination angle δ with respect to the (x,y) plane.

We adopt an orientation of coordinates and an origin of time such that the line of nodes coincides with, and the secondary is on, the x-axis at time t = 0. We denote the position vector of the secondary star by \mathbf{D} with $D \equiv |\mathbf{D}|$.

The total gravitational potential Ψ due to the binary at a point with position vector \mathbf{r} is given by:

$$\Psi = -\frac{GM_p}{|\mathbf{r}|} - \frac{GM_s}{|\mathbf{r} - \mathbf{D}|} + \frac{GM_s \mathbf{r} \cdot \mathbf{D}}{D^3},\tag{1}$$

where G is the gravitational constant. The first dominant term is due to the primary, while the remaining perturbing terms are due to the secondary. The last indirect term accounts for the acceleration of the origin of the coordinate system.

We are interested in disk warps that are excited by terms in the potential that are odd in z and have azimuthal mode number m=1 when a Fourier analysis in φ is carried out. The terms in the expansion of the potential that are of the required form are given by:

$$\Psi' = \frac{\sin \varphi}{2\pi} \int_0^{2\pi} \left[\Psi(r, \varphi', z, \omega t) - \Psi(r, \varphi', -z, \omega t) \right] \sin \varphi' d\varphi'.$$
(2)

We consider a thin disk such that $z \ll r$. Since $r \ll D$, we then retain only the lowest order terms in r/D and z/D in the above integral, which becomes:

$$\Psi' = -\frac{3}{4} \frac{GM_s}{D^3} rz \left[(1 - \cos \delta) \sin \delta \sin \left(\varphi + 2\omega t \right) \right]$$

$$-(1+\cos\delta)\sin\delta\sin(\varphi-2\omega t) + \sin 2\delta\sin\varphi]. \quad (3)$$

Because the principle of linear superposition can be used, the general problem may be reduced to calculating the response to a complex potential of the form:

$$\Psi' = i frz e^{i(\varphi - \Omega_p t)}. \tag{4}$$

Here the pattern frequency Ω_p of the perturber is one of 0, 2ω or -2ω , and f is an appropriate real amplitude.

3. BASIC EQUATIONS

The response of the disk is determined by the equation of continuity:

$$\frac{\partial \rho}{\partial t} + \boldsymbol{\nabla} \cdot (\rho \mathbf{v}) = 0, \tag{5}$$

and the equation of motion:

$$\frac{\partial \mathbf{v}}{\partial t} + (\mathbf{v} \cdot \nabla) \mathbf{v} = \frac{1}{\rho} (-\nabla P + \mathbf{F}_{\nu}) - \nabla \Psi, \tag{6}$$

where P is the pressure, ρ is the mass density and \mathbf{v} is the flow velocity. We allow for the possible presence of a viscous force \mathbf{F}_{ν} but, following Papaloizou & Lin (1995), we shall assume that it does not affect the undistorted axisymmetric disk so that it operates on the perturbed flow only. This approximation is justified because the disk viscous timescale is much longer than the characteristic timescales of the processes we are interested in here (in particular, bending waves propagate with a velocity comparable to the sound speed, so that the waves crossing time is much shorter than the viscous timescale).

For simplicity, we adopt a polytropic equation of state:

$$P = K\rho^{1+1/n},\tag{7}$$

where K is the polytropic constant and n is the polytropic index. The sound speed is then given by $c_s^2 = dP/d\rho$.

4. EQUILIBRIUM STRUCTURE OF THE DISK

We adopt the same model as in Papaloizou & Terquem (1995). Namely we suppose that the equilibrium disk is axisymmetric and in a state of differential rotation such that, in cylindrical coordinates, the flow velocity is given by $\mathbf{v} = (0, r\Omega, 0)$. For a barotropic equation of state, the angular velocity Ω is a function of r alone.

For a thin disk under the influence of a point mass, integration of the vertical hydrostatic equilibrium equation gives (Papaloizou & Terquem 1995):

$$H(r) = \left(\frac{\left[2K(1+n)\right]^n}{C_n}\right)^{1/(2n+1)} \left(\Sigma \Omega_K^{-2n}\right)^{1/(2n+1)}, \quad (8)$$

$$\rho(r,z) = \left[2K(1+n)C_n^2\right]^{-n/(2n+1)}$$

$$\times \left(\Sigma \Omega_K\right)^{2n/(2n+1)} \left(1 - \frac{z^2}{H^2}\right)^n. \tag{9}$$

Here Ω_K is the Keplerian angular velocity given by $\Omega_K^2 = GM_p/r^3$, H is the disk semi–thickness, Σ is the surface mass density defined by:

$$\Sigma(r) = \int_{-H(r)}^{H(r)} \rho(r, z) dz,$$

and

$$C_{n} = \frac{\Gamma\left(\frac{1}{2}\right)\Gamma\left(n+1\right)}{\Gamma\left(\frac{1}{2}+n+1\right)},$$

where Γ denotes the gamma function.

It then follows from the radial hydrostatic equilibrium equation that the angular velocity is given by:

$$\Omega^{2} = \Omega_{K}^{2} + \frac{1}{r} \left\{ \frac{\left[K \left(1+n\right)\right]^{2n}}{2C_{n}^{2}} \right\}^{1/(2n+1)}$$

$$\times \frac{\partial}{\partial r} \left[\left(\Sigma \Omega_{K}\right)^{2/(2n+1)} \right]. \tag{10}$$

In principle, the surface density profile should be determined self–consistently as a result of viscous diffusion (Lynden–Bell & Pringle 1974). However, since we ignore the effect of viscosity on the unperturbed disk, we are free to specify arbitrary density profiles for the equilibrium disk model. For Σ we then take a function that is constant in the main body of the disk with a taper to make it vanish at the outer boundary:

$$\Sigma(r) = \Sigma_0 \frac{\sigma(r)}{[1 + \sigma(r)^q]^{1/q}},\tag{11}$$

which approximates $\Sigma(r) = \Sigma_0 \min[1, \sigma(r)]$ with

$$\sigma(r) = \left\{1 - \left[\frac{r - (R - \Delta)}{\Delta}\right]^p\right\}^N.$$

The parameters Δ , which represents the width of the taper interior to the outer boundary, N, q and p are constrained such that the square of the epicyclic frequency, which is defined by:

$$\kappa^2 = \frac{2\Omega}{r} \frac{d\left(r^2\Omega\right)}{dr},$$

is positive everywhere in the disk. For the numerical calculations we take $N=\left(2n+1\right)/2,\,\Delta/R=0.1,\,q=4$ and p=1.

The polytropic constant K is determined by specifying a maximum value of the relative semi-thickness, H/r, in

the disk, and the fiducial surface mass density Σ_0 is fixed by specifying the total mass M of the disk.

Figure 1 shows the surface mass density, Σ , the relative semi–thickness, H/r, the ratio of the sound speed to the Keplerian frequency, $c_s/\Omega_K \sim H$, and the ratio of the epicyclic frequency to the Keplerian frequency, κ/Ω_K , versus the radius r for the equilibrium disk models described above with $M=10^{-2}M_p$ and $(H/r)_{max}=0.1$. The epicyclic frequency departs from Ω_K at the outer edge of the disk because of the abrupt decrease of Σ there.

5. THE DISK RESPONSE

5.1. Linear Perturbations

In this paper we consider small perturbations, so that the basic equations (5) and (6) can be linearized. As the relevant linearization of the equations has already been discussed by Papaloizou & Lin (1995), we provide only an abbreviated discussion here. We denote Eulerian perturbations with a prime. Because the perturbing potential, Ψ' , is proportional to $exp\left[i\left(\varphi-\Omega_p t\right)\right]$, the φ and t dependence of the induced perturbations is the same. We denote with a tilde the part of the Eulerian perturbations that depends only on r and z. For instance, the Eulerian perturbed radial velocity is denoted v'_r , and we have $v'_r(r,\varphi,z,t)=\tilde{v}'_r(r,z)exp\left[i\left(\varphi-\Omega_p t\right)\right]$.

We define a quantity g (the physical meaning of which will be given at the end of this section) through:

$$\frac{P'}{\rho} + \Psi' = -irz\Omega^2 g,\tag{12}$$

and we also have $g(r, \varphi, z, t) = \tilde{g}(r, z) exp [i (\varphi - \Omega_p t)].$

It was first shown by Papaloizou & Pringle (1983) that horizontal motions induced in a near Keplerian tilted disk are resonantly driven. The main effect of a small viscosity is then to act on the vertical shear in the horizontal perturbed velocities $\partial v_r'/\partial z$ and $\partial v_\varphi'/\partial z$. Demianski & Ivanov (1997) and Ivanov & Illarionov (1997) have recently given the relativistic generalization of this effect. Following Papaloizou & Lin (1995), we then retain only the horizontal components of the viscous force perturbation:

$$F'_{\nu r} = \frac{\partial}{\partial z} \left(\rho \nu_{\rm v} \frac{\partial v'_r}{\partial z} \right), \quad F'_{\nu \varphi} = \frac{\partial}{\partial z} \left(\rho \nu_{\rm v} \frac{\partial v'_\varphi}{\partial z} \right), \tag{13}$$

where $\nu_{\rm v}$ is the kinematic viscosity that couples to the vertical shear. This approximation is accurate when $\alpha_{\rm v} \ll 1$. The numerical calculations have actually shown that, when $\alpha_{\rm v}$ becomes larger than 0.1, the terms that are neglected in this approximation become comparable to the terms that are retained. For this reason, we shall limit our numerical calculations to values of $\alpha_{\rm v}$ smaller than 0.1.

Here we have assumed that the disk is turbulent and that dissipation can be modeled as a turbulent viscosity. The most likely mechanism for producing such a turbulent viscosity is the magnetorotational Balbus–Hawley instability (Balbus & Hawley 1991). We note however that this instability may not operate in all the parts of protostellar disks (Balbus & Hawley 1998). Also, it is not clear that the tidal waves would be damped by the turbulent viscosity in the way described by equations (13). In this

formulation, we implicitly assume that the turbulent viscosity is not affected by the tidally–produced velocities, which is not necessarily true. However, since the wavelength of the tidal waves we consider is much larger than the disk semi–thickness, this formulation may be correct.

Papaloizou & Lin (1995) have shown that when the radial wavelength of the perturbations is larger than the disk semi–thickness, a vertical averaging approximation, in which \tilde{g} is assumed to be independent of z, can be used. Each of \tilde{v}'_r and \tilde{v}'_φ are then proportional to z, with \tilde{v}'_z being independent of z. They have found some support for the procedure in a numerical study of the propagation of disturbances in disk models that take the vertical structure fully into account.

Linearization of the equation of motion followed by multiplication by ρz and vertical averaging then gives the velocity perturbations in the form:

$$\frac{\tilde{v}_r'}{\Omega z} = -\left(1 - \Omega_p/\Omega\right) \tilde{g} + \frac{\left(1 - \Omega_p/\Omega\right) r \frac{d\tilde{g}}{dr} + \tilde{g} \left(3 - \Omega_p/\Omega\right) \Omega_p^2/\Omega^2}{\left(1 - \Omega_p/\Omega - i\alpha_v\right)^2 - \kappa^2/\Omega^2},$$
(14)

$$\frac{\tilde{v}_{\varphi}'}{\Omega z} = \frac{i}{1 - \Omega_p/\Omega} \left(\tilde{g} + \frac{\kappa^2}{2\Omega^2} \frac{\tilde{v}_r'}{\Omega z} \right), \tag{15}$$

$$\frac{\tilde{v}_z'}{r\Omega} = \frac{\tilde{g}}{1 - \Omega_p/\Omega},\tag{16}$$

where $\alpha_{\rm v}$ is a vertical average of the standard Shakura & Sunyaev (1973) parameter that couples to the vertical shear. It is defined by:

$$\alpha_{\rm v} = \int_{-\infty}^{\infty} \rho \nu_{\rm v} dz / \left(\Omega \int_{-\infty}^{\infty} \rho z^2 dz \right). \tag{17}$$

As mentioned above, the main effect of viscosity is to damp the resonantly driven horizontal velocities. Therefore, the viscous terms which do not act directly on the resonance have been neglected. This is consistent with keeping only the components of the viscous force given by equation (13). Again, this is accurate only when $\alpha_{\rm v} \ll 1$.

The same procedure applied to the continuity equation gives:

$$-i\left(\Omega - \Omega_p\right)\mathcal{I} + \frac{\Omega^2 \tilde{g}}{(\Omega - \Omega_p)} \left\{ r \left[(\Omega - \Omega_p)^2 - \Omega^2 \right] \mathcal{J} + \frac{d\mu}{dr} \right\}$$

$$= -\frac{1}{r} \left[\frac{\partial}{\partial r} \left(r \mu \frac{\tilde{v}_r'}{z} \right) + i \mu \frac{\tilde{v}_{\varphi}'}{z} \right], \tag{18}$$

in which

$$\mathcal{J} = \int_{-\infty}^{+\infty} \frac{\rho z^2}{c^2} dz, \; \mu = \int_{-\infty}^{+\infty} \rho z^2 dz, \; \mathcal{I} = \int_{-\infty}^{+\infty} \frac{\rho z}{c^2} \tilde{\Psi}' dz.$$

We note that equation (18) depends on the viscosity only through the perturbed velocities.

To close the system of equations, we need a relation between \tilde{P}' and $\tilde{\rho}'$. For simplicity, we assume that the equation of state is the same for the perturbed and unperturbed flows. Linearization of the equation of state (7) then gives

$$\tilde{P}' = c_s^2 \tilde{\rho}'. \tag{19}$$

We now give a physical interpretation of g. Equation (16) can be used to express \tilde{g} in terms of the vertical Lagrangian displacement $\tilde{\xi}_z$:

$$\tilde{g} = i \left(1 - \Omega_p / \Omega\right)^2 \frac{\tilde{\xi}_z}{r},\tag{20}$$

where again we have defined $\tilde{\xi}_z$ such that $\xi_z(r, \varphi, z, t) = \tilde{\xi}_z(r, z) exp [i (\varphi - \Omega_p t)].$

When $\Omega_p \ll \tilde{\Omega}$, the physical relative vertical displacement is then given by:

$$Re\left(\frac{\xi_z}{r}\right) = Re(\tilde{g})\sin\left(\varphi - \Omega_p t\right) + Im(\tilde{g})\cos\left(\varphi - \Omega_p t\right).$$
 (21)

Thus, when $\Omega_p = 0$, $Re(\tilde{g})$ and $Im(\tilde{g})$ are the relative vertical displacement along the y and x-axis respectively. We note that a constant value of \tilde{g} corresponds to a rigid tilt.

5.2. Zero-Frequency Response

From equation (3), we have to consider the disk response to a secular potential perturbation with zero forcing frequency. When $\Omega_p = 0$ and $\alpha_{\rm v} \ll 1$, equations (14), (15), (16) and (18) reduce to the single second-order ordinary differential equation for \tilde{g} (Papaloizou & Lin 1995):

$$\frac{d}{dr} \left[\frac{\mu}{\left(1 - i\alpha_{\rm v}\right)^2 - \kappa^2/\Omega^2} \frac{d\tilde{g}}{dr} \right] = \frac{i\mathcal{I}}{r}.$$
 (22)

Here we have assumed that:

$$\mu \ll Re \left\{ r \frac{d}{dr} \left[\frac{\mu}{\left(1 - i\alpha_{\rm v}\right)^2 - \kappa^2/\Omega^2} \right] \right\},$$
 (23)

which is certainly a reasonable approximation for $\alpha_{\rm v} \ll 1$.

It can be shown that with the term \mathcal{I} in its present form, the x-component of the torque is non zero. This torque leads to the precession of the disk, as in a gyroscope. By writing the equation of motion for $\Omega_p = 0$ in the frame defined in § 2, we have assumed that the response of the disk appears steady in a nonrotating frame. Because of the precessional motion induced by the secular perturbation, the response is actually steady in a frame rotating with the precession frequency. The Coriolis force corresponding to this additional motion must then be added in the equation of motion (the centrifugal force can be neglected since it is of second order in the precession frequency). The magnitude of the Coriolis force in the frame in which the response appears steady has to be such that the xcomponent of the total torque (involving both the Coriolis and the gravitational forces) is zero.

This requirement leads to the expression of the precession frequency ω_p (Papaloizou & Terquem 1995; see also Kuijken 1991 in the context of galactic disks):

$$\frac{\omega_p}{\Omega_0} = -\frac{3}{4} \frac{M_s}{M_s + M_p} \left(\frac{\omega}{\Omega_0}\right)^2 \cos \delta \times \int_{r_{in}}^R \frac{\Sigma}{(\Omega/\Omega_0)^2} dr / \int_{r_{in}}^R \frac{\Sigma}{\Omega/\Omega_0} dr , \quad (24)$$

where $\Omega_0 = \Omega(R)$ and r_{in} is the disk inner boundary. Here the disk has been assumed to precess as a rigid body. This is expected if the disk can communicate with itself, either through wave propagation or viscous diffusion (selfgravity being ignored), on a timescale less than the precession period. As long as α_{ν} is smaller than the disk aspect ratio H/r (which is almost constant throughout most of the disk), bending waves may propagate (Papaloizou & Pringle 1983; Papaloizou & Lin 1995). The ability of these waves to propagate throughout the disk during a precession time implies approximately that $H/r > |\omega_p|/\Omega_0$. This is the condition for near rigid body precession in an inviscid disk (Papaloizou & Terquem 1995). The numerical simulations of Larwood et al. (1996) show that this condition also holds in a viscous disk in which $\alpha_{\rm v}$ does not exceed H/r. This indicates that in the absence of selfgravity, as long as $\alpha_{\rm v} < H/r$ (which is likely to be satisfied in protostellar disks), pressure is the factor that controls the efficiency of communication throughout the disk and then the precessional behavior of the disk. A more complete discussion of the precession of warped disks (which includes self-gravity) is given by Papaloizou et al. (1998).

The Coriolis force can be taken into account by replacing $\tilde{\Psi}'$ with:

$$\tilde{\Psi}' + 2i\omega_p rz\Omega sin\delta. \tag{25}$$

For the zero–frequency case, $\tilde{\Psi}'$ will represent the total term (25) and the real amplitude f will represent $f + 2\omega_p\Omega\sin\delta$ from now on.

With this new definition of f, \tilde{g} is then given by:

$$\tilde{g}\left(r\right) = -\int_{r_{in}}^{r} \frac{\left(1 - i\alpha_{v}\right)^{2} - \kappa^{2}/\Omega^{2}}{\mu} \int_{r_{in}}^{r'} \mathcal{J}\left(r''\right) f\left(r''\right) dr'' dr',$$
(26)

where the quantity in the outer integral has to be evaluated at the radius r'. We have supposed that $\tilde{g} = 0$ at $r = r_{in}$, but we note that an arbitrary constant may be added to \tilde{g} . This corresponds to an arbitrarily small rigid tilt that we assume eliminated by the choice of coordinate system.

The above expression shows that, depending on whether $\alpha_{\rm v}$ is larger or smaller than $1 - \kappa^2/\Omega^2 \sim H^2/r^2$, the imaginary part of \tilde{g} is larger or smaller than its real part, respectively. According to equation (21), this corresponds to a vertical displacement produced by the secular response being mainly along the x- or y-axis, respectively.

We finally comment that the above treatment is accurate only when $|\omega_p|/\Omega_0$ is smaller than the maximum of $1-\kappa^2/\Omega^2\sim H^2/r^2$ and $\alpha_{\rm v}$. If this is not the case, then the precession frequency has to be taken into account in the resonant denominator $(1-i\alpha_{\rm v})^2-\kappa^2/\Omega^2$ where it would be the dominant term.

5.3. Finite-Frequency Response

We now consider the response generated in the disk by those terms in the perturbing potential with finite forcing frequency. When $\Omega_p \neq 0$, the second-order differential equation for \tilde{g} obtained from equations (14), (15), (16) and (18) takes on the general form:

$$A\frac{d^2\tilde{g}}{dr^2} + B\frac{d\tilde{g}}{dr} + C\tilde{g} = S, \tag{27}$$

with

$$A = \frac{r\left(\Omega - \Omega_p\right)}{D_2}\mu,\tag{28}$$

$$B = \mu \Omega \left\{ \frac{1}{D_2} \left[\left(1 + r \frac{d \ln \mu}{d r} \right) D_1 - \frac{\kappa^2}{2\Omega^2} + \left(3 - \frac{\Omega_p}{\Omega} \right) \frac{\Omega_p^2}{\Omega^2} \right] \right\}$$

$$-D_1 + \frac{1}{\Omega} \frac{d}{dr} \left(\frac{D_1 r \Omega}{D_2} \right) \right\}, \tag{29}$$

$$S = i \left(\Omega - \Omega_p \right) \mathcal{I}, \tag{30}$$

where we have set $D_1 = 1 - \Omega_p/\Omega$ and $D_2 = (1 - \Omega_p/\Omega - i\alpha_v)^2 - \kappa^2/\Omega^2$. By introducing the function h such that:

$$\frac{1}{h}\frac{dh}{dr} = \frac{1}{A}\left(B - \frac{dA}{dr}\right),\tag{31}$$

equation (27) can be recast in the form:

$$\frac{d}{dr}\left(hA\frac{d\tilde{g}}{dr}\right) + hC\tilde{g} = hS,\tag{32}$$

the solutions of which are given by the Green's function method:

$$\tilde{g}\left(r\right) = \frac{1}{W} \left[g_1\left(r\right) \int_{r_{in}}^{r} g_2\left(r'\right) s\left(r'\right) dr' \right]$$

$$+g_{2}(r)\int_{r}^{R}g_{1}(r')s(r')dr'$$
 (33)

Here $s = h (\Omega - \Omega_p) fr \Sigma \Omega^{-2}$, W is the constant

$$W = hA \left(g_1 \frac{dg_2}{dr} - \frac{dg_1}{dr} g_2 \right), \tag{34}$$

and g_1 and g_2 are the solutions of the homogeneous differential equation that satisfy the outer and inner boundary conditions respectively. In the numerical calculations presented below, g_1 and g_2 are calculated directly from equations (14), (15) and (18) using the fourth-order Runge–Kutta procedure with adaptative stepsize control given by Press et al. (1986). Computation of the function h then allows \tilde{g} to be calculated from (33).

5.4. Boundary Conditions

Equation (27) has a regular singularity at the outer edge r=R (see Papaloizou & Terquem 1995). Our outer boundary condition is thus that the solution be regular there

We take the inner boundary to be perfectly reflective. The radial velocity in spherical polar coordinates, $(r\tilde{v}'_r + z\tilde{v}'_z)/(r^2 + z^2)^{1/2}$, thus vanishes at the locations (r,z) such that $r^2 + z^2 = r_{in}^2$, where r_{in} is the disk inner radius. Using the expression (16) of \tilde{v}'_z , this means that at these locations:

$$rz\left[\frac{\tilde{v}_r'}{z} + \frac{\Omega\tilde{g}}{1 - \Omega/\Omega_p}\right] = 0, \tag{35}$$

and then, by continuity:

$$\frac{\tilde{v}_r'}{z} + \frac{\Omega \tilde{g}}{1 - \Omega/\Omega_p} = 0, \tag{36}$$

at the inner boundary.

We note that for the largest values of α_v , we expect the waves to be damped before reaching the center of the disk, such that the results are independent of the inner boundary condition. For $\alpha_v=0$, since there is no dissipation at the boundaries, we expect no torque to be exerted on the disk and no net angular momentum flux to flow through its boundaries.

5.5. Domain of Validity of This Analysis

In this analysis, we have neglected the variation of \tilde{g} with z. As noted above, Papaloizou & Lin (1995) have shown that this approximation is valid when the scale of variation of \tilde{g} with radius is larger than the disk semi–thickness H, i.e. when

$$\left| \frac{1}{\tilde{q}} \frac{d\tilde{g}}{dr} \right| < \frac{1}{H}. \tag{37}$$

When this is not satisfied, dispersive effects, which have been neglected here, should be taken into account.

Since we also consider linear waves, our analysis is valid as long as the perturbed velocities are smaller than the sound speed. When they become supersonic, shocks occur that damp the waves (Nelson & Papaloizou 1998). However, it is not correct to compare the Eulerian perturbed velocities given by the equations (14), (15) and (16) with the sound speed to know whether the waves are linear or not. This is because the system should be invariant under the addition of a rigid tilt (i.e. a constant) to \tilde{g} . An increase of \tilde{g} corresponding to the addition of a rigid tilt could make the Eulerian perturbed velocities larger than the sound speed without the waves getting nonlinear. In principle, as pointed out by Papaloizou & Lin (1995), to get perturbed quantities that do not depend on the addition of a rigid tilt (i.e. that depend only on the radial gradient of \tilde{q}), we should use Lagrangian rather than Eulerian variables. However, since the Eulerian perturbed radial velocity in spherical polar coordinates depends only on the gradient of \tilde{q} in the limit of small perturbing frequency, we can compare this quantity to the sound speed to decide whether the motion is subsonic. The criterion that has to be satisfied is then:

$$\left| \frac{rv_r' + zv_z'}{(r^2 + z^2)^{1/2}} \right| \simeq \left| \frac{\Omega z r \frac{dq}{dr}}{(1 - \Omega_p/\Omega - i\alpha_v)^2 - \kappa^2/\Omega^2} \right| < c_s,$$
(38)

where we have assumed that $\Omega_p \ll \Omega$ and $z \ll r$. We have kept Ω_p/Ω in the resonant denominator because, even though this term is small compared with unity, it may still be larger than $1 - \kappa^2/\Omega^2$.

The WKB dispersion relation for bending waves gives $\Omega_p = (c_s/2) k$ where $k \sim 1/R$ is the wavenumber (Papaloizou & Lin 1995). For finite perturbing frequency, we can then rewrite the above criterion in the form:

$$\delta \tilde{g} < \max\left(\frac{H}{r}, \alpha_{\rm v}\right),$$
 (39)

where $\delta \tilde{g}$ is the variation of the tilt angle across the disk and we have used the fact that $1-\kappa^2/\Omega^2 \sim H^2/r^2 < H/r$. By H/r we mean the aspect ratio anywhere in the disk, since this quantity does not vary significantly throughout the disk. For $\Omega_p=0$, the condition we get is:

$$\delta \tilde{g} < \max\left(\frac{H^2}{r^2}, \alpha_{\rm v}\right)$$
 (40)

As pointed out in § 5.2, depending on whether $\alpha_{\rm v}$ is larger or smaller than $1-\kappa^2/\Omega^2$, the imaginary part of \tilde{g} is larger or smaller than its real part, respectively. Therefore, the above criterion and equation (21) tell us that the variation across the disk of the relative vertical displacement produced by the secular perturbation is limited by $\alpha_{\rm v}$ along the x-axis and by H^2/r^2 along the y-axis.

We note that in an inviscid disk, the zero–frequency perturbation produces $\delta \tilde{g} \sim |\omega_p|/\Omega(R)$ (Papaloizou, Korycansky & Terquem 1995). Since, as we have pointed out in § 5.2, our analysis is valid only when $|\omega_p|/\Omega(R)$ is smaller than the maximum of H^2/r^2 and α_v , the above criterion is always satisfied in an inviscid disk.

The most likely situation in a protostellar disk corresponds to $\alpha_{\rm v} < H/r$. In that case, when the perturbed velocities are close to the sound speed, the secular perturbation produces a steady (in the precessing frame) tilt the variation of which across the disk is on the order of H^2/r^2 or $\alpha_{\rm v}$, whichever term is the largest. Superposed on this steady tilt, bending waves produced by the finite frequency terms propagate, corresponding to a tilt the variation of which across the disk is on the order of H/r. This is exactly what was observed in the SPH simulations performed by Larwood & Papaloizou (1997), in which $\alpha_{\rm v}$ was larger than H^2/r^2 . We note that since in the case of protostellar disks H/r is likely to be close to 0.1, the variation of the vertical displacement across the disk due to the nonsecular tidal perturbations can be as large as about a tenth of the disk radius while the perturbation remains linear.

6. ANGULAR MOMENTUM EXCHANGE

Tidal perturbation of a disk may lead to an exchange of angular momentum between the disk and the perturber.

If the disk is inviscid and does not contain any corotation resonance, the nature of the boundaries would determine whether such an exchange takes place or not (see Lin &

Papaloizou 1993 for example). Because of the conservation of wave action in an inviscid disk, waves excited at the outer boundary propagate through the disk with an increasing amplitude if the disk surface density increases inward or is uniform (see Lightill 1978 for example). It is usually assumed that they become non linear before reaching the center and are dissipated through interaction with the background flow. Thus, the inner boundary can be taken to be dissipative (Papaloizou & Terquem 1995). Dissipation at the boundary then introduces a phase lag between the perturber and the disk response, enabling a net torque to be exerted by the perturber. This torque is transferred to the disk through dissipation of the waves at the boundary. Because of the conservation of angular momentum, the net torque is equal to the difference of angular momentum flux through the disk boundaries. This flux is constant (independent of r) inside the disk, since there is not dissipation there.

The situation is different when a corotation resonance is present in the disk, since this singularity provides a location where angular momentum can be absorbed or emitted (Goldreich & Tremaine 1979; Goldreich & Nicholson 1989).

When the disk is viscous, its response is not in phase with the perturber. A net torque is then exerted on the disk even if the boundaries are reflective, and the angular momentum flux inside the disk is not constant, since the perturbed velocities are viscously dissipated. This situation has been investigated by Papaloizou & Pringle (1977) and Papaloizou & Lin (1984) in the context of coplanar orbit. Here we present the analysis corresponding to a non coplanar orbit.

We note that whenever the perturber rotates outside the disk, the torque exerted on the disk is negative. Through dissipation of the waves, the disk then loses angular momentum. We first derive an expression of the torque in terms of \tilde{g} , and then relate it to $\alpha_{\rm v}$ using angular momentum conservation.

6.1. Expression for the Torque

The net torque exerted by the perturber on the disk is given by:

$$\mathbf{T} = -\int_{V} Re \left[\rho + \tilde{\rho}' e^{i(\varphi - \Omega_{p} t)} \right] \mathbf{r}$$

$$\times Re \left[\nabla \left(\tilde{\Psi}' e^{i(\varphi - \Omega_{p} t)} \right) \right] dV, \tag{41}$$

where the integration is over the volume V of the unperturbed disk. Because of the φ -periodicity, the first-order term is zero, and the z-component of the torque is then

$$T_z = -\int_V Re \left[\tilde{\rho}' e^{i(\varphi - \Omega_p t)} \right] Re \left[\frac{\partial}{\partial \varphi} \left(\tilde{\Psi}' e^{i(\varphi - \Omega_p t)} \right) \right] dV, \tag{42}$$

which is equivalent to

$$T_z = \frac{1}{2} Im \left(\int_V \tilde{\rho}'^* \tilde{\Psi}' dV \right). \tag{43}$$

Using equations (12) and (19), $\tilde{\rho}'$ in the above equation can be replaced in terms of \tilde{g} . The expression of T_z then

involves \mathcal{J} , which, in a Keplerian disk, is equal to $\Sigma\Omega^{-2}$. We then get

$$T_{z} = \pi \int_{r_{in}}^{R} Im\left(\tilde{g}\right) f \Sigma r^{3} dr \tag{44}$$

where f is the real amplitude defined by (4) (which has to be modified when $\Omega_p = 0$ in order to take into account the disk precession, see § 5.2). In the numerical calculations presented below, the torque T_z will be computed from this expression.

If J_D is the total angular momentum of the disk, the tidal effects we have considered would remove the angular momentum content of the disk on a timescale

$$t_d = \frac{J_D}{T_z} \sim \frac{4}{5} \frac{M\sqrt{GM_pR}}{T_z}.$$
 (45)

We shall compare this timescale with the viscous timescale $t_{\nu,h} \sim (r/H)^2 \Omega(R)^{-1}/\alpha_h$ where we will take $H/r = (H/r)_{max}$ (for our disk models, H/r does not vary by more than 20% in the main body of the disk, as indicated in Fig. 1). Here α_h is the viscous parameter that couples to the horizontal shear.

We also define the torque integral $T_z(r)$, which is the torque exerted between the inner boundary and the radius r:

$$T_z(r) = \pi \int_{r_{in}}^{r} Im(\tilde{g}) f \Sigma r^3 dr.$$
 (46)

6.2. Angular Momentum Conservation

To get the angular momentum conservation equation, which is of second order in the perturbed quantities, we first take the Lagrangian perturbation of the equation of motion (6) and multiply by the unperturbed mass density. To first order, this leads to (Lynden–Bell & Ostriker 1967):

$$\rho \left[\frac{\partial^2 \pmb{\xi}}{\partial t^2} + \Omega^2 \frac{\partial^2 \pmb{\xi}}{\partial \varphi^2} + \pmb{\Omega} \times (\pmb{\Omega} \times \pmb{\xi}) + 2\Omega \frac{\partial^2 \pmb{\xi}}{\partial \varphi \partial t} + 2 \pmb{\Omega} \times \frac{\partial \pmb{\xi}}{\partial t} \right]$$

$$+2\Omega \mathbf{\Omega} \times \frac{\partial \boldsymbol{\xi}}{\partial \varphi} = \rho \Delta \left(-\frac{1}{\rho} \boldsymbol{\nabla} P \right) + \mathbf{F'}_{\nu} - \rho \boldsymbol{\nabla} \Psi' - \rho \left(\boldsymbol{\xi} \cdot \boldsymbol{\nabla} \right) \boldsymbol{\nabla} \Psi.$$
(47)

Here, ξ is the Lagrangian displacement vector, Δ denotes the Lagrangian change operator, and we have used the relation between Lagrangian and Eulerian perturbations of a quantity Q to first order in ξ :

$$\Delta Q = Q' + (\boldsymbol{\xi} \cdot \boldsymbol{\nabla}) Q. \tag{48}$$

The vector $\mathbf{\Omega} \equiv \Omega \hat{\mathbf{k}}$, with $\hat{\mathbf{k}}$ being the unit vector in the z-direction. To derive equation (47), we have used the fact that at equilibrium $\mathbf{F}_{\nu} = \mathbf{0}$.

We now take the scalar product of equation (47) with $\boldsymbol{\xi}^*$, which is the complex conjugate of $\boldsymbol{\xi}$. Since $\partial/\partial t = -i\Omega_p$ and $\partial/\partial\varphi = i$, all the terms on the left hand side of the resulting equation are real. We then take the imaginary part of this equation and integrate it over the volume V of the unperturbed disk. This leads to:

$$Im \left\{ \int_{V} \left[\boldsymbol{\xi}^{*} \cdot \mathcal{P} \left(\boldsymbol{\xi} \right) + \boldsymbol{\xi}^{*} \cdot \mathbf{F'}_{\nu} \right] \right.$$

$$-\rho \boldsymbol{\xi}^* \cdot \boldsymbol{\nabla} \Psi' - \rho \boldsymbol{\xi}^* \cdot (\boldsymbol{\xi} \cdot \boldsymbol{\nabla}) \boldsymbol{\nabla} \Psi | dV \} = 0, \tag{49}$$

where we have defined the linear operator \mathcal{P} such that $\mathcal{P}(\boldsymbol{\xi}) = \rho \Delta \left(-\nabla P/\rho\right)$. We note that if the terms on the left hand side of equation (47) had non zero contribution to equation (49), it would be related to the total time derivative of the perturbed specific angular momentum of the disk.

Using the perturbed equation of state (19) in the form $\Delta P/P = (1+1/n) \Delta \rho/\rho$, it can be shown (Lynden–Bell & Ostriker 1967) that:

$$\int_{V} \boldsymbol{\xi}^{*} \cdot \mathcal{P}\left(\boldsymbol{\xi}\right) dV = B + \int_{V} \boldsymbol{\xi}^{*} \cdot \mathcal{O}\left(\boldsymbol{\xi}\right) dV, \qquad (50)$$

where \mathcal{O} is a self–adjoint linear operator, and B is a boundary term:

$$B = \int_{S} \left[\frac{1}{n} \rho \left(\nabla \cdot \boldsymbol{\xi} \right) \boldsymbol{\xi}^* + P \left(\boldsymbol{\xi}^* \cdot \nabla \right) \boldsymbol{\xi} \right] \cdot \mathbf{n} \, dS.$$
 (51)

The integration is over the surface S of the disk, and \mathbf{n} is the unit vector perpendicular to this surface, oriented toward the disk exterior. Since P and ρ vanish at r=R and $z=\pm H$ and we consider models for which $r_{in}\simeq 0$, we have B=0. In addition, since $\mathcal O$ is self-adjoint, the integral on the right hand side of equation (50) is real. The term involving $\mathcal P$ in equation (49) is then zero.

Using the fact that $\partial^2 \Psi / \partial r \partial z = \partial^2 \Psi / \partial z \partial r$, it can also be shown that the term involving $\nabla \Psi$ is zero.

Since equation (49) has no φ and t-dependence, we can now use the tilded variables again. We define $\tilde{\boldsymbol{\xi}}$ such that $\boldsymbol{\xi}(r,\varphi,z,t) = \tilde{\boldsymbol{\xi}}(r,z) exp\left[i\left(\varphi-\Omega_p t\right)\right]$. We define $\tilde{\boldsymbol{\xi}}^*$ similarly. The term involving $\tilde{\Psi}'$ in equation (49) can be written as follows:

$$Im\left(\int_{V} \rho \tilde{\boldsymbol{\xi}}^{*} \cdot \boldsymbol{\nabla} \tilde{\boldsymbol{\Psi}}' dV\right)$$
$$= Im\left(\int_{V} \boldsymbol{\nabla} \cdot \left(\rho \tilde{\boldsymbol{\xi}}^{*} \tilde{\boldsymbol{\Psi}}'\right) dV\right) + Im\left(\int_{V} \tilde{\boldsymbol{\Psi}}' \tilde{\rho}'^{*} dV\right), \quad (52)$$

where an integration by parts has been performed and the linearized continuity equation:

$$\tilde{\rho}' = -\nabla \cdot \left(\rho \tilde{\boldsymbol{\xi}}\right),\tag{53}$$

(see, for example, Tassoul 1978) has been used. The first term on the right-hand side of equation (52) is zero because ρ vanishes at r=R and $z=\pm H$ and $r_{in}\simeq 0$. Equation (49) then becomes:

$$Im\left(\int_{V} \tilde{\rho}'^{*} \tilde{\Psi}' dV\right) = Im\left(\int_{V} \tilde{\xi}^{*} \cdot \tilde{\mathbf{F}}'_{\nu} dV\right). \tag{54}$$

From equation (43), we see that this is equivalent to:

$$T_z = Im\left(\pi \int_{r_{in}}^R \int_{-H}^H \tilde{\xi}^* \cdot \tilde{\mathbf{F}}'_{\nu} r dr dz\right).$$
 (55)

We now use the relation between the Eulerian velocity perturbation and the Lagrangian displacement:

$$\tilde{\mathbf{v}}' + (\tilde{\boldsymbol{\xi}} \cdot \boldsymbol{\nabla}) \mathbf{v} = \frac{\partial \tilde{\boldsymbol{\xi}}}{\partial t} + (\mathbf{v} \cdot \boldsymbol{\nabla}) \tilde{\boldsymbol{\xi}}$$
 (56)

together with the expression (13) of $\tilde{\mathbf{F}}'_{\nu}$, the relation (17) and the fact that $\rho(\pm H) = 0$ to transform equation (55) into:

$$T_z = -\pi \int_{r_{in}}^{R} \mu \alpha_{\mathbf{v}} r \frac{\left|\tilde{v}_r'/z\right|^2 + \left|\tilde{v}_{\varphi}'/z\right|^2}{1 - \Omega_p/\Omega} dr$$

$$-\pi Im \left[\int_{r_{in}}^{R} \mu \alpha_{v} r \frac{\left(\tilde{v}_{r}^{\prime *}/z\right) \left(\tilde{v}_{\varphi}^{\prime}/z\right)}{\left(1 - \Omega_{p}/\Omega\right)^{2}} \left(1 - \frac{\kappa^{2}}{2\Omega^{2}}\right) \right]. \quad (57)$$

In the numerical calculations presented below, the torque will be computed from equation (44) and compared with the result of the above equation.

In a Keplerian disk, $\kappa \simeq \Omega$. Then, when $\Omega_p \ll \Omega$ and $\alpha_v \ll 1$, equation (15) is well approximated by:

$$\frac{\tilde{v}_{\varphi}'}{z} \simeq i \frac{\kappa^2}{2\Omega^2} \frac{\tilde{v}_r'}{z},\tag{58}$$

so that T_z can be approximated by:

$$T_z \simeq -\frac{3\pi}{2} \int_{r_{in}}^{R} \mu \alpha_{\rm v} r \left| \frac{\tilde{v}_r'}{z} \right|^2 dr.$$
 (59)

As expected, the torque is negative. Here we consider linear perturbations such that the perturbed velocities remain smaller than the sound speed. We have pointed out in § 5.5 that, since the system should be invariant under the addition of a rigid tilt to \tilde{g} , it is not in principle correct to compare the Eulerian perturbed velocities to the sound speed to know whether the waves are linear or not. However, since the dominant term in the expression (14) of \tilde{v}'_r is the term proportional to the gradient of \tilde{g} , we can compare this velocity to the sound speed to decide whether the motion is subsonic. Therefore we can get an estimate of the maximum value of the torque by setting $|\tilde{v}'_r| \sim c_s$, $\mu \sim \rho H^3$ and dropping the integration. This leads to a minimum value of t_d which is equal to $t_{\nu,h} \times \alpha_h/\alpha_v$. Only if α_v were larger than α_h could t_d be smaller than $t_{\nu,h}$.

An other useful quantity for interpreting our results is the flux of vertical angular momentum in the radial direction at radius r:

$$J(r) = \int_{z=-H}^{H} \int_{\varphi=0}^{2\pi} \rho r^2 Re\left(v_{\varphi}'\right) Re\left(v_{r}'\right) d\varphi dz, \qquad (60)$$

which can also be written

$$J(r) = \pi \mu r^2 Re \left[\frac{\tilde{v}_{\varphi}'}{z} \left(\frac{\tilde{v}_{r}'}{z} \right)^* \right]. \tag{61}$$

The torque $T_z(r)$ exerted between the radii r_{in} and r results in a change of angular momentum of the disk. Part of this angular momentum is advected through the boundaries (this is $J(r) - J(r_{in}) \simeq J(r)$ since $r_{in} \simeq 0$), and part is dissipated between these radii. Thus the quantity $T_z(r) - J(r)$ is the amount of angular momentum deposited in the disk between the inner boundary and the radius r.

As we shall see, this quantity is negative, which means that the disk loses angular momentum.

In the numerical calculations presented below, the torque integral will be computed from equation (46) and J(r) will be computed directly from the velocities using equations (14) and (15).

7. NUMERICAL RESULTS

We compute the torque exerted on protostellar disks by a perturber with an orbit that is inclined to the plane of the disk. For a coplanar system, one expects the circumprimary disk to be truncated by tidal effects in such a way that its radius is not greater than about one—third of the separation of the system (Papaloizou & Pringle 1977). Larwood et al. (1996) have shown that tidal truncation is only marginally affected by the lack of coplanarity. Thus in our models we adopt $D \geq 3R$. Since we consider binary mass ratio of unity $(M_s = M_p)$, the perturbing potential is small compared with the potential of the central star, justifying the assumption of small perturbation.

For computational convenience, we normalize the units such that $M_p = 1$, R = 1, and $\Omega_K(R) = 1$. Apart for the calculation of the epicyclic frequency, the rotation law in the disk is taken to be Keplerian (the departure from the Keplerian law, which occurs mainly at the disk outer edge, does not exceed $\sim 3\%$). The inner boundary of the disk is $r_{in} = 10^{-4}$, and the outer boundary is taken to be $r_{out} = 0.99$ rather than 1 in order to avoid a zero surface mass density at the outer edge.

We present here the results of some disk response calculations for an inclination $\delta = \pi/4$, a polytropic index n=1.5 and a disk mass $M=10^{-2}$. Results for an arbitrary inclination $\delta < \pi/2$ (prograde orbit) or $\pi/2 < \delta < \pi$ (retrograde orbit) can be obtained straightforwardly since T_z (and then $1/t_d$) corresponding to $\Omega_p=\pm 2\omega$ and 0 is proportional to $(1\pm\cos\delta)^2\sin^2\delta$ and $\sin^22\delta$, respectively. As shown by equation (24), the precession frequency scales with $\cos\delta$. Since g is independent of M (see equations [14], [15], [16] and [18]), expression (44) shows that $T_z \propto M$. The quantities ω_p , t_d and $t_{\nu,h}$ are independent of M.

7.1. Uniform $\alpha_{\rm v}$

In table 1 we summarize the results obtained for different values of the parameters, which are the separation of the system D, the viscous parameter $\alpha_{\rm v}$ and the maximum value of the relative semi–thickness of the disk $(H/r)_{max}$. The quantities we compute are the torque T_z associated with each of the perturbing frequencies 2ω (prograde term), -2ω (retrograde term) and 0, the disk precession frequency ω_p and the ratio of the tidal timescale t_d to the viscous timescale $t_{\nu,h}$. We have taken here $\alpha_h = \alpha_{\rm v}$. The two values of the torque have been computed using equations (44) and (57), the result corresponding to equation (57) being in parentheses. The timescale t_d is computed from equation (45) with T_z being the sum of the contributions from each frequency.

We note that when either one of the criterions (37) or (38) is not satisfied (cases indicated by a footnote), it is always close to the disk outer edge. This is because the density varies more rapidly there than in the other parts of the disk. Also the scale of variation of \tilde{g} never becomes smaller than H by less than a factor of a few. Similarly,

when the radial velocity in spherical polar coordinates becomes larger than the sound speed, it is only by a factor of a few. We note that the results we present in this case can still be used since the perturbed quantities can be reduced by choosing appropriate scaling parameters, like the initial inclination δ or the mass of the disk M.

In all cases the condition $|\omega_p|/\Omega(R) < \max(H^2/r^2, \alpha_v)$ is satisfied (see § 5.2). The condition for near rigid body precession, $H/R \gg |\omega_p|/\Omega(R)$, is also always satisfied.

We note that there is a good agreement between the values of the torque given by equations (44) and (57). In addition, in the cases we computed, we found this latter equation to be very well approximated by (59).

To simplify the discussion, we note T_z^+ , T_z^- and T_z^0 the torque associated respectively with $\Omega_p=2\omega$, -2ω and 0. Furthermore, we separate the δ -dependence by writing $T_z^{\pm}=T_{\pm}(1\pm\cos\delta)^2\sin^2\delta$ and $T_z^0=T_0\sin^22\delta$ with T_{\pm} and T_0 being independent of δ .

Since part of this section is devoted to the tilt \tilde{g} , we recall that \tilde{g} is related to the relative vertical displacement through equation (21). When $\Omega_p = 0$, $Re(\tilde{g})$ and $Im(\tilde{g})$ are the relative vertical displacement along the y and x-axis respectively.

7.1.1. Finite-Frequency Response

Figure 2 shows the real and imaginary parts of \tilde{g} versus r for models 2 and $\Omega_p = 2\omega$ (figures for $\Omega_p = -2\omega$ are similar). We see that the wave-like character of the disk response disappears when $\alpha_{\rm v}$ becomes larger than H/r(which is 0.05 in these models). This is in agreement with Papaloizou & Pringle (1983) and Papaloizou & Lin (1995) (and also with the relativistic generalization of Demianski & Ivanov 1997 and Ivanov & Illarionov 1997) who have shown that, in a near Keplerian disk (self-gravitating or not), the longest wavelength disturbances undergo a transition between wave-like and diffusive behavior when $\alpha_{\rm v} \sim H/r$. We note, however, that when $\alpha_{\rm v} \geq H/r$, there are still some oscillations in the half outer part of the disk. This is because bending waves have a long wavelength, such that they can still penetrate relatively far before being diffused out.

The magnitude of $Re(\tilde{g})$ does not vary with $\alpha_{\rm v}$, since it is controlled mainly by the radial pressure force. On the contrary, the magnitude of $Im(\tilde{g})$ is much more sensitive to the viscosity, although it does not vary monotonically with $\alpha_{\rm v}$.

By comparing models 2a and 3c and also models 2c and 4c, which differ only by the value of $(H/r)_{max}$, we have checked that the wavelength of the response is proportional to H/r. This is expected since bending waves propagate with a velocity which, being half the sound speed, is proportional to H/r, and the wavelength is proportional to the wave velocity.

In all the cases we have computed, except model 3f, $T_z^+ \geq T_z^-$, but $T_- \geq T_+$, in agreement with Papaloizou & Terquem (1995). In general, the shorter the wavelength of the response, the smaller the torque, and the wave corresponding to the retrograde term has a slightly longer wavelength than that corresponding to the prograde term. The difference between T_+ and T_- (and T_0) is still significant for the largest values of the separation computed here. We expect all these quantities to converge toward

the same value when 2ω approaches 0, which probably means here $2\omega/\Omega(R)\ll\alpha_{\rm v}$ since the torque is controlled by viscosity. This is not satisfied even for model 3i which has $2\omega/\Omega(R)=0.09$. However, we observe that the difference between these torques is reduced from a factor 9 to a factor less than 4 when model 3i is run with $\alpha_{\rm v}=0.1$.

In Figure 3 the net torque T_z is plotted versus D in a semi-log representation for $\alpha_{\rm v}=10^{-3}$ (models 3 plus other values of D) and $\alpha_{\rm v}=10^{-2}$ (models 4 plus other values of D) and for $\Omega_p=\pm 2\omega$ and 0. Before commenting on the resonances, we note that the torque associated with the finite frequency terms out of resonance does not decrease when the separation increases up to $D \sim 8$. This confirms the results of Papaloizou & Terquem (1995). There are competing effects acting when the separation of the system is increased. On the one hand, the wavelength of the tidal waves becomes larger (since it is inversely proportional to its frequency), which tends to increase the torque. On the other hand, the amplitude of the perturbing potential decreases, which tends to reduce the torque. It seems that the first effect is dominant for $D \leq 8$. It seems like the torque begins to decrease with the separation when the wavelength becomes comparable to the disk radius, which happens for $D \sim 9$. This is reasonable since the wavelength cannot increase further.

In Figure 3 we can see resonances, which occur when the frequency of the tidal waves is equal to that of some free normal global bending mode of the disk, and cause the torque to become very large, even infinite if there is no dissipation (Papaloizou & Lin 1984). In a resonance, the torque indeed increases when $\alpha_{\rm v}$ decreases, in contrast to what is observed out of resonance. It seems that there is no longer any resonance for D>10. This would not be surprising since the wavelength of the response is then comparable to the disk radius. A more detailed description of the resonance which occurs at $D\sim8.5$ is given in the Appendix.

Since the resonances depend on the spectrum of the free normal bending modes of the disk, they are model—dependent. In particular, they occur only if the the waves can be at least partially reflected at the inner boundary, otherwise there is no free normal global bending mode in the disk (see also Hunter & Toomre 1969 for the case of a purely self–gravitating disk).

The values of the torque displayed in Figure 3 correspond to $\delta = \pi/4$. However, for this particular value of δ , the perturbed velocities may become larger than the sound speed close to a resonance. These values of the torque should then be scaled to be used for other values of δ , or for other disk parameters. For $\alpha_{\rm v} = 10^{-2}$, the resonances are very weak, indicating that the waves are almost completely dissipated before reaching the disk inner boundary.

We have compared our results with those obtained by Papaloizou & Terquem (1995) for an inviscid disk in which the inner boundary is dissipative. Remembering that they had $\delta = \pi/2$, we found that, in general, we could reproduce their results with $\alpha_{\rm v} \sim 10^{-2}$. This confirms that, when $\alpha_{\rm v} \sim 10^{-2}$, the waves are dissipated before reaching the disk inner boundary.

Out of resonance, the torque T_z^{\pm} associated with the finite frequency terms is proportional to α_v as long as this

parameter is smaller than some critical value. Then, for the larger values of $\alpha_{\rm v}$, T_z^{\pm} is independent of the viscosity. This is in agreement with the theoretical expectation (Goldreich & Tremaine 1982) and the work of Papaloizou & Terquem (1995). We indeed expect the torque to be independent of whatever dissipation acts in the disk providing the waves are dissipated before reaching the disk inner boundary. If the waves are reflected on the disk inner boundary, the situation is more complicated because the angular momentum carried by the waves has a different sign depending on whether the waves are in-going or outgoing. Therefore part of the angular momentum lost by the disk while the waves propagate inwards is given back by the waves propagating outwards. The net amount of angular momentum lost by the disk then depends on how efficiently the waves are reflected. Using this argument, we then find that, when H/r = 0.1 and 0.05, the waves are damped before reaching the disk inner boundary when $\alpha_{\rm v}$ is larger than $\sim 5\times 10^{-2}$ and $\sim 5\times 10^{-3}$, respectively (for H/r = 0.1, this is a bit larger than the value found above). Such a dependence of this critical value of $\alpha_{\rm v}$ with H/r is expected. Indeed, the shorter the wavelength, the more easily are the waves dissipated. Since the wavelength is proportional to H/r (see above), we then expect that for a given $\alpha_{\rm v}$ dissipation is more efficient for small values of H/r. For the same reason, the net torque T_z^{\pm} increases with H/r (see models 3c and 2a and models 4c and 2c). The coupling between the response and the perturbing potential is indeed more efficient when the response has a long wavelength, and the integral in equation (44) from which the torque is calculated is then larger.

7.1.2. Zero-Frequency Response

Figure 4 shows the real and imaginary parts of \tilde{g} versus r for models 2 and $\Omega_p = 0$. As expected, we observe that the zero–frequency response is not wave–like.

From equation (26) we see that, as long as $\alpha_{\rm v}^2 \ll 1 - \kappa^2/\Omega^2 \sim H^2/r^2$, which is the case for $\alpha_{\rm v} \leq 10^{-2}$, $Re(\tilde{g})$ is almost independent of the viscosity. When $\alpha_{\rm v} = 0.1$, $\alpha_{\rm v}^2$ dominates over $1 - \kappa^2/\Omega^2$, and since it appears in the expression of $Re(\tilde{g})$ with the minus sign, $Re(\tilde{g})$ becomes negative. The particular behavior of $Re(\tilde{g})$ in the outer parts of the disk is produced by the fact that the surface mass density drops to zero there, thus increasing $1 - \kappa^2/\Omega^2$. As expected from equation (26), $Im(\tilde{g})$ is proportional to $\alpha_{\rm v}$.

Papaloizou, Korycansky & Terquem (1995) computed the real part of \tilde{g} for an inviscid disk with an equilibrium state similar to that we have set up here and for $\Omega_p = 0$ and D = 7. We have checked that the results we get for the smallest values of α_v are in complete agreement with theirs.

Equation (44) shows that T_z depends only on $Im(\tilde{g})$, not on $Re(\tilde{g})$. Since for the secular response $Im(\tilde{g}) \propto \alpha_{\rm v}$, T_z^0 is also proportional to $\alpha_{\rm v}$. This is borne out by the numerical results. Also equation (26) indicates that $\tilde{g} \propto 1/H^2$. Thus if we vary H/r while keeping Σ constant, we get from equation (44) that $T_z \propto 1/H^2$. This is confirmed by models 3c and 2a and models 4c and 2c, which differ only by the value of $(H/r)_{max}$. This is in contrast to the finite frequency response, for which the torque increases with H/r (see above).

Figure 3 indicates that $T_z^0 \gg T_z^{\pm}$ out of resonance. Since

we also have $T_0 \gg T_{\pm}$, T_z^0 is always going to be much larger than T_z^{\pm} for δ not too close to $\pi/2$ (typically for $\delta < 70^{\circ}$ or $110^{\circ} < \delta < 180^{\circ}$).

In contrast to the finite frequency response, the zero-frequency response is not wave-like, and we then expect T_z^0 to decrease continuously with D. This is indeed what we observe in Figure 3.

7.1.3. Angular Momentum Dissipation as a Function of Radius

Figures 5 and 6 show $T_z(r)-J(r)$ normalized to unity versus r for various models. This represents the angular momentum deposited in the disk between the inner boundary and the radius r. The fact that this quantity is negative means that the disk loses angular momentum. Of course, $|T_z(r)-J(r)|$ should increase with r. However, we observe in Figure 5 that for D=3 and $\Omega=2\omega$ this function has a little 'hump' close to the disk outer edge. We interpret it as being a numerical effect, since its amplitude is found to depend on the accuracy of the calculations.

We first observe that bending waves are able to transport a significant fraction of the negative angular momentum they carry deep into the inner parts of the disk. For the parameters corresponding to model 1b, Figure 5 shows that the retrograde and prograde waves transport respectively 35% and 60% of the total negative angular momentum they deposit into the disk at radii smaller than 0.3 and 0.4 respectively. In contrast, only 20\% of the total negative angular momentum carried by the zero-frequency perturbation is deposited at radii smaller than 0.4. We note however that, out of resonance, the net amount of angular momentum deposited at small radii by the $\Omega_p = 0$ perturbation is not necessarily smaller than that deposited by the finite frequency perturbations. Also, the fraction of angular momentum deposited close to the disk outer edge by the finite frequency responses (especially the retrograde wave) is larger than that deposited by the secular response.

It appears that the secular response gets dissipated very progressively throughout the disk, whereas the prograde and retrograde waves are dissipated preferentially at some locations in the disk. The position of these locations seems to depend on the wavelength of these waves.

The resonances do not affect the distribution of dissipation of angular momentum in the disk, although they obviously increase the absolute value of the actual amount of angular momentum deposited. This is due to the fact that the magnitude of the response, not its wavelength, is affected by a resonance.

In Figure 6 we have plotted $T_z(r)-J(r)$ versus r for $\Omega_p=-2\omega$ and different values of $\alpha_{\rm v}$. We see clearly on these plots the transition that occurs when $\alpha_{\rm v}\sim H/r$. When $\alpha_{\rm v}$ becomes larger than H/r, the wave–like response of the disk disappears. Thus, the curves corresponding to $\Omega_p=-2\omega$ have a shape similar to those corresponding to the secular response.

In general, when α_v is increased, the fraction of negative angular momentum deposited at small radii decreases. This is expected since the waves, excited predominantly in the outer parts of the disk, get dissipated more easily at large radii when α_v is large.

We observe in Figure 6.a that there is hardly any difference between the cases $\alpha_{\rm v}=10^{-4}$ and $\alpha_{\rm v}=10^{-3}$. This means that whatever the amount of angular momentum transported by the wave, the same fraction is deposited between r_{in} and r in both cases. This probably indicates that the wave is able to reach the disk inner boundary for these values of $\alpha_{\rm v}$. For larger $\alpha_{\rm v}$ for which the wave is completely dissipated before reaching the inner boundary, no angular momentum is deposited at small radii, so that the curves look different. This indicates that, for $(H/r)_{max} = 0.1$, the waves do not reach the inner boundary when $\alpha_{\rm v}$ is larger than $\sim 10^{-2}$. For $(H/r)_{max}=0.05$ (Figure 6.b), the critical value of $\alpha_{\rm v}$ above which the waves do not reach the inner boundary is between 10^{-3} and 5×10^{-3} . These values are in agreement with those found above. Our calculations also show that a larger fraction of the negative angular momentum is deposited at small radii when H/ris decreased. However, we have checked that this effect is less significant when the distance interior to the outer boundary occupied by the taper of the surface mass density is reduced along with the semi-thickness.

7.2. Nonuniform α_v

We have run model 1c with a nonuniform viscosity $\alpha_{\rm v}=10^{-2}x^5$ and $\alpha_{\rm v}=10^{-2}\left(1-x\right)^5$. These models correspond to a disk where respectively the inner and outer parts are nonviscous.

Figure 7.a shows the imaginary part of \tilde{g} versus r for $\Omega_p = 0$ corresponding to these viscosity laws. The uniform $\alpha_{\rm v}$ case is also plotted for comparison. The real part of \tilde{q} is not shown since it does not depend on $\alpha_{\rm v}$ for these small values of the viscosity (see discussion above). We see that when the outer parts of the disk are nonviscous, $Im(\tilde{q})$ in the inner parts is similar to the uniform $\alpha_{\rm v}$ case, while it has an almost constant value in the outer parts. When the inner parts of the disk are nonviscous, $Im(\tilde{q})$ is almost zero there, while it is significant in the outer parts. This behavior can be understood by remembering that $Im[\tilde{g}(r)]$ is the integral from r_{in} to r of a function proportional to $\alpha_{\rm v}$ (see equation [26]). Since $Im(\tilde{g})$ varies less through the disk than in the uniform α_v case, \tilde{v}'_r given by equation (14) is smaller. This, together with a smaller $\alpha_{\rm v}$, leads to a smaller net torque given by equation (59).

When $\Omega_p \neq 0$, there is not such a difference between the uniform and nonuniform α_v cases. The torque is smaller in the nonuniform case, but $Im(\tilde{g})$ does not change significantly from one case to the other. The reason is probably that $Im(\tilde{g})$ does not vary monotonically with α_v , as shown in Figure 2.

Figure 7.b shows $T_z(r) - J(r)$ versus r for the same models and $\Omega_p = 0$. We observe that, as expected, no angular momentum is deposited at radii where α_v is very small (small radii for $\alpha_v \propto x^5$ and large radii for $\alpha_v \propto (1-x)^5$).

8. DISCUSSION

In this paper, we have calculated the response of a viscous gaseous disk to tidal perturbations with azimuthal mode number m=1 and odd symmetry in z with respect to the equatorial plane for both zero and finite perturbing frequencies. We concentrated on these types of perturbations because they arise for inclined disks and they lead to

a long–wavelength response. The effects of perturbations with even symmetry, which occur in the coplanar case, may be superposed on the effects of those with the odd symmetry.

Since the response of a viscous disk is not in phase with the perturbing potential, a tidal torque is exerted on the disk. When the perturber rotates outside the disk, this torque results in a decrease of the disk angular momentum. Part of the (negative) angular momentum of the perturbation is carried by tidal waves away from the location where the torque is exerted, and part is dissipated locally through viscous interaction of the waves with the background flow.

We have shown that the tidal torque is comparable to the horizontal viscous stress acting on the background flow when the perturbed velocities in the disk are on the order of the sound speed c_s . If these velocities remain subsonic, the tidal torque can exceed the horizontal viscous stress only if the parameter $\alpha_{\rm v}$ which couples to the vertical shear is larger than the parameter $\alpha_{\rm h}$, which is coupled to the horizontal shear. We note that, so far, there is no indication about whether these two parameters should be the same or not. Nelson & Papaloizou (1998) have found that, when the perturbed velocities exceed c_s , shocks reduce the amplitude of the perturbation such that the disk moves back to a state where these velocities are smaller than c_s . When shocks occur, the tidal torque exerted on the disk may become larger than the horizontal viscous stress.

We have found that, in protostellar disks, bending waves are able to propagate and transport a significant fraction of the negative angular momentum they carry in the disk inner parts. This is due to their relatively large wavelength. Therefore, tidal interactions in noncoplanar systems may not be confined to the regions close to the disk outer edge where the waves are excited. For the disk models we have set up, which extends down to the stellar surface, the value of $\alpha_{\rm v}$ above which the waves get dissipated before reaching the disk inner boundary varies between 5×10^{-3} and 10^{-2} for a disk aspect ratio between 0.05 and 0.1 (this critical value of $\alpha_{\rm v}$ increases with the disk semi-thickness). We note that if we had set up an annulus rather than a disk, the surface mass density would drop at the inner boundary. Then, for small $\alpha_{\rm v}$, the waves would have a tendency to become nonlinear and then to dissipate before reaching the inner boundary. Thus, the behavior of bending waves could be similar in an annulus with small $\alpha_{\rm v}$ and in a disk with larger $\alpha_{\rm v}$. In the limit of small viscosity, dissipation could also occur as a result of parametric instabilities (Papaloizou & Terquem 1995; C.F. Gammie, J.J. Goodman & G.I. Ogilvie 1998, private communication), the effect of which may be to lead to a larger effective $\alpha_{\rm v}$. However, since the waves we consider here propagate in a nonuniform medium, it is not clear whether they would be efficiently damped by these instabilities.

It the disk model allows at least partial reflection from the center, the tidal interaction becomes resonant when the frequency of the tidal waves is equal to that of some free normal global bending mode of the disk. For the equilibrium disk models we have considered, we have found that a particularly strong resonance occurs when the separation is about 8.5 times the disk radius. The torque

associated with the finite frequency terms then increases by many orders of magnitude. However the response may be limited by shocks and nonlinear effects. The strength of the resonance is inversely proportional to $\alpha_{\rm v}$. In our calculations, the range of separation for which the torque is significantly increased is rather large, which means that the effects of tidal interaction, like disk truncation, may occur even when the separation of the binary is large. In addition to this strong resonance we have found a few other resonances with different strengths and widths. From these calculations, it appears that the probability for the interaction to be resonant may be significant. However, these results depend on the particular equilibrium disk models we have set up.

We note that the disk is expected to be truncated such that the inner Lindblad (2:1) resonance with the companion, which could provide effective wave excitation, is more or less excluded from the disk.

Out of resonance, we find that the torque associated with the zero–frequency perturbing term is much larger than that associated with the finite frequency terms. Of course, if the separation of the system is large enough (at least 10 times the disk radius in our models), the difference between finite frequency and secular terms disappears. When the secular response is dominant, the tidal torque is proportional to $\alpha_{\rm v}$ in the limit $\alpha_{\rm v} \ll 1$. This has the consequence that the ratio of the tidal timescale t_d (time that would be required for the tidal effects we have considered to remove the angular momentum content of the disk) to the disk viscous timescale $t_{\nu,\rm h}$ is proportional to $\alpha_{\rm h}/\alpha_{\rm v}$.

What observable effects would these tidal interactions produce in protostellar disks? First, as we mentioned in the introduction, they would lead to the precession of the jets that originate from these disks. The precession timescale that we can infer from the observation of jets that are modeled as precessing is consistent with this motion being induced by tidal effects in binary systems (Terquem et al. 1998).

Also, as we have already pointed out in § 5.5, the secular perturbation produces a tilt the variation of which can be up to $\alpha_{\rm v}$ along the line of nodes and H^2/r^2 along the direction perpendicular to the line of nodes. Superposed on this steady (in the precessing frame) tilt, there is a tilt produced by the finite frequency perturbations, the variation of which across the disk can be up to H/r. Such asymmetries in the outer parts of protostellar disks could be observed. Because the variations along the line of nodes and along the perpendicular to the line of nodes depend on $\alpha_{\rm v}$ and H/r, respectively, observations of warped protostellar disks have the potential to give important information about the physics of these disks.

Protostellar disks are believed to be rather thick, i.e. $H/r \sim 0.1$. Our calculations show that for such an aspect ratio, the viscosity above which bending waves are damped before reaching the central star is $\alpha_{\rm v} \sim 10^{-2}$. Observations seem to indicate that $\alpha_{\rm h}$ in protostellar disks is on the order of 10^{-3} – 10^{-2} . If $\alpha_{\rm v}$ is smaller than or comparable to 10^{-2} , resonances may occur, as described above, providing the disk inner edge allows some reflection of the waves. In that case, we could observe truncated disks with sharp edges even when the binary separation is large. If

 $\alpha_{\rm v}$ is larger than but close to 10^{-2} , bending waves are still able to propagate throughout most of the disk. In addition, given that protostellar disks are rather thick, these waves propagate fast (they cross the disk on a time comparable to the sound crossing time). In that case, it may be possible to observe some time–dependent phenomena with a frequency equal to twice the orbital frequency.

In the case of protostellar disks, comparison between observations and theory is now becoming possible. A noncoplanar binary system, HK Tau, has been observed for the first time very recently (see \S 1.1), and subsequent work will be devoted to interpreting these observations. In the meantime, we can comment briefly on some observations related to X–ray binaries.

There is evidence from the light curve of X–ray binaries, such as Hercules X–1 and SS 433, that their associated accretion disks may be in a state of precession in the tidal field of the binary companion. Katz (1980a, 1980b) has indicated that the observed precession periods of these two systems are consistent with the precession being induced by the tidal field of the secondary.

In the case of SS 433, it is interesting to note that an additional "nodding" motion with a period half the orbital period is observed (see Margon 1984 and references therein). Katz et al. (1982) suggested that this nodding motion is produced by the gravitational torque exerted by the companion. In their model, the nodding is viscously transmitted from the outside, where the torque is significant, to the interior, where the jets are seen to respond to the motion. This implies an extremely large viscosity in the disk.

Here we point out that the observed period of this motion is consistent with the nodding being produced by bending waves. As these waves propagate with the sound speed and the disk is observed to be very thick (Margon 1984), they could transmit the motion through the disk on a timescale comparable to its dynamical timescale. For the waves to reach the disk interior, $\alpha_{\rm v}$ would have to be smaller than H/r. It is not clear that this condition is satisfied here. The disk viscosity would then probably have to be smaller than that predicted by the model of Katz et al. (1982).

We finally observe that a rapid communication time through the disk also makes problems with the radiation—driven warping model proposed by Maloney & Begelman (1997) to explain the precession of the disk in SS 433. In this model, the communication between the different parts of the disk, which is assumed to occur because of viscosity alone, is on a timescale that is characteristic for mass to flow through the disk. It is therefore very slow since the viscous timescale must be long for the warping instability to occur (Pringle 1996).

It is a pleasure to thank John Papaloizou for his advice, encouragement, and many valuable suggestions and discussions. I acknowledge Steve Balbus, Doug Lin, Jim Pringle and Michel Tagger for very useful comments on an earlier draft of this paper, and John Larwood for pointing out the "nodding" motion in SS 433. I also thank an anonymous referee whose comments helped to improve the quality of this paper. This work was supported by the Center for Star Formation Studies at NASA/Ames Re-

search Center and the University of California at Berkeley and Santa Cruz. I am grateful to the Isaac Newton Insti-

tute at Cambridge University for support during the final stages of this work.

APPENDIX

We describe here in more detail the resonance that occurs at $D \sim 8.5$, since it is particularly strong. For $\Omega_p = 2\omega$ and -2ω , resonance occurs at D = 8.25 and D = 8.425 respectively. We observe that, for the values of α_v considered here, the range of D for which the torque is significantly increased is rather large. We see that the strength of the resonance is proportional to α_v^{-1} . This is expected since the strength of the resonance is inversely proportional to the damping factor, which itself is proportional to α_v when dissipation is due to viscosity. We also note that the integral of the torque over the range of frequencies in this resonance is independent of α_v . This can be understood in the following way. For $\Omega_p = 2\omega$ (the same argument would apply for $\Omega_p = -2\omega$), the torque at or close to resonance can be written

$$T_z = \frac{-\mathcal{A}\alpha_{\rm v}}{4\left(\bar{\omega} - \bar{\omega}_0\right)^2 + \alpha_{\rm v}^2},\tag{1}$$

where $\bar{\omega} = \omega/\Omega(R)$, ω_0 is the resonant frequency and \mathcal{A} is an amplitude which does not depend on α_v . We have calculated that $\mathcal{A} \simeq 8 \times 10^{-11}$. For the values of α_v considered, we have checked that the integral of the torque from $\bar{\omega}_0 - \Delta \bar{\omega}$ to $\bar{\omega}_0 + \Delta \bar{\omega}$ does not depend very much on whether $2\Delta \bar{\omega}$ is taken to be the range of frequencies in the resonance or for which expression (1) is valid (the latter being smaller). We then approximate the integral I of the torque over the resonance by using (1), so that

$$I = -A Arctan \frac{2\Delta\bar{\omega}}{\alpha_{\rm v}}.$$
 (2)

For $\alpha_{\rm v} = 10^{-3}$ or 10^{-4} , the range of frequencies $2\Delta\bar{\omega}$ for which (1) is valid is large compared with $\alpha_{\rm v}$, so that $I \simeq -\mathcal{A}\pi/2$, independent of $\alpha_{\rm v}$. For $\alpha_{\rm v} = 10^{-2}$, although $2\Delta\bar{\omega}$ is only a few times $\alpha_{\rm v}$, this relation is still valid within a factor less than 2 (due to the rapid convergence of the function Arctan).

REFERENCES

in preparation

Artymowicz, P. 1994, ApJ, 423, 581
Balbus, S. A., & Hawley, J. F. 1991, ApJ, 376, 214
Balbus, S. A., & Hawley, J. F. 1998, Rev. Mod. Phys., 70, 1
Bardeen, J. M., & Petterson, J. A. 1975, ApJ, 195, L65
Bibo, E. A., The, P. S., & Dawanas, D. N. 1992, A&A, 260, 293
Böhm, K.-H., & Solf, J. 1994, ApJ, 430, 277
Corporon, P., Lagrange, A.-M., & Beust, H. 1996, A&A, 310, 228
Davis, C. J., Mundt, R., & Eislöffel, J. 1994, ApJ, 437, L55
Demianski, M. & Ivanov, P. B. 1997, A&A, 324, 829 Demianski, M., & Ivanov, P. B. 1997, A&A, 324, 829
Dutrey, A., Guilloteau, S., & Simon, M. 1994, A&A, 286, 149
Edwards, S., Cabrit, S., Strom, S. E., Heyer, I., Strom, K. M., & Anderson, E. 1987, ApJ, 321, 473 Goldreich, P., & Nicholson P. D. 1989, ApJ, 342, 1075 Goldreich, P., & Tremaine, S. 1978, Icarus, 34, 240 Goldreich, P., & Tremaine, S. 1979, ApJ, 233, 857 Goldreich, P., & Tremaine, S. 1982, ARA&A, 20, 249 Heller, C. H. 1995, ApJ, 455, 252 Hunter, C., & Toomre, A. 1969, ApJ, 155, 747 Ivanov, P. B., & Illarionov, A. F. 1997, MNRAS, 285, 394 Jensen, E. L. N., Mathieu, R. D., & Fuller, G. A. 1996, ApJ, 458, Katz, J. I. 1980a, ApJ, 236, L127 Katz, J. I. 1980b, Astrophysical Letters, 20, 135 Katz, J. I., Anderson, S. F., Margon, B., & Grandi, S. A. 1982, ApJ, 260, 780 Kuijken, K. 1991, ApJ, 376, 467 Larwood, J. D. 1997, MNRAS, 290, 490 Larwood, J. D., Nelson, R. P., Papaloizou, J. C. B., & Terquem, C. 1996, MNRAS, 282, 597 Larwood, J. D., & Papaloizou, J. C. B. 1997, MNRAS, 285, 288 Lightill, J. 1978, Waves in Fluids (Cambridge: Cambridge Univ. Press) Lin, D. N. C., & Papaloizou, J. C. B. 1993, in Protostars and Planets III, ed. E. H. Levy & J. Lunine (Tucson: Univ. Arizona Press), Lynden-Bell, D., & Ostriker, J. P. 1967, MNRAS, 136, 293 Lynden-Bell, D., & Pringle, J. E. 1974, MNRAS, 168, 603 Maloney, P. R., & Begelman, M. C. 1997, ApJ, 491, L43 Margon, B. 1984, ARA&A, 22, 507 Masset, F., & Tagger, M. 1996, A&A, 307, 21

Mathieu, R. D. 1994, ARA&A, 32, 465

McCaughrean, M. J., & O'Dell, C. R. 1996, AJ, 111, 1977

Nelson, R. P., & Papaloizou, J. C. B. 1998, MNRAS, submitted

Ostriker, E. C. 1994, ApJ, 424, 292

Paczyński, B. 1977, ApJ, 216, 822

Papaloizou, J. C. B., Korycansky, D. G., & Terquem, C. 1995, Ann. of the New York Ac. of Sc., 773, 261

Papaloizou, J. C. B., & Lin, D. N. C. 1984, ApJ, 285, 818

Papaloizou, J. C. B., & Lin, D. N. C. 1995, ApJ, 438, 841

Papaloizou, J. C. B., & Pringle, J. E. 1977, MNRAS, 181, 441

Papaloizou, J. C. B., & Pringle, J. E. 1983, MNRAS, 202, 1181

Papaloizou, J. C. B., & Terquem, C. 1995, MNRAS, 274, 987

Papaloizou, J. C. B., & Terquem, C., & Lin, D. N. C. 1998, ApJ, 497, 212

Petterson, J. A. 1977, ApJ, 218, 783

Press, W. H., Flannery, B. P., Teukolsky, S. A., Vetterling, W. T. 1986, Numerical Recipes: The Art of Scientific Computing (Cambridge: Cambridge University Press)

Pringle, J. E. 1996, MNRAS, 281, 811

Roddier, C., Roddier, F., Northcott, M. J., Graves, J. E., & Jim, K. 1996, ApJ, 463, 326

Shakura, N. I., & Sunyaev, R. A. 1973, A&A, 24, 337

Shu, F. H. 1984, in Planetary Rings, ed. R. Greenberg & A. Brahic (Tucson: Univ. Arizona Press), 513

Shu, F. H., Cuzzi, J. N., & Lissauer, J. J. 1983, Icarus, 53, 185

Sparke, L. S., & Casertano, S. 1988, MNRAS, 234, 873

Stapelfeldt, K. R., Krist, J. E., Ménard, F., Bouvier, J., Padgett, D. L., & Burrows, C. J. 1998, ApJ Letters, in press

Stauffer, J. R., Prosser, C. F., Hartmann, L., & McCaughrean, M. J. 1994, AJ, 108, 1375

Steiman—Cameron, T. Y., & Durisen, R. H. 1988, ApJ, 325, 26

Tassoul, J.—L. 1978, Theory of rotating stars (Princeton: Princeton Univ. Press)

Terquem, C., & Bertout, C. 1993, A&A, 274, 291

Terquem, C., & Bertout, C. 1996, MNRAS, 279, 415

Terquem, C., Eislöffel, J., Papaloizou, J. C. B., & Nelson, R. P. 1998, Terquem, C., Eislöffel, J., Papaloizou, J. C. B., & Nelson, R. P. 1998, Terquem, C., Eislöffel, J., Papaloizou, J. C. B., & Nelson, R. P. 1998, Terquem, C., Eislöffel, J., Papaloizou, J. C. B., & Nelson, R. P

Toomre, A. 1983, in IAU Symp. 100. Internal Kinematics and Dy-

namics of Galaxies, ed. E. Athanassoula (Dordrecht: Reidel), 177

Table 1: Torque and Corresponding Tidal Evolution Timescale.

Label	D	$lpha_{ m v}$	$\left(\frac{H}{r}\right)_{max}$	T_z			ω_p	$t_d/t_{\nu,\mathrm{h}}$
			· / max	-2ω	-2ω	0	(10^{-2})	
1a	3	10^{-4}	0.1	$-4(3) \times 10^{-12}$ a	$-2(0.8) \times 10^{-12}$	$-1(1) \times 10^{-9}$ b	-1.1	5.9
1b	_	10^{-3}	_	$-4(3) \times 10^{-11}$ a	$-2(0.7) \times 10^{-11}$	$-1(1) \times 10^{-8}$ b	_	_
1c	_	10^{-2}	_	$-3(2) \times 10^{-10}$ a	$-1(0.5) \times 10^{-10}$	$-1(1) \times 10^{-7}$ c	-	_
1d	_	0.1	-	$-9(8) \times 10^{-10}$ a	$-4(2) \times 10^{-10}$	$-1(1) \times 10^{-6}$ c	-	-
2a	6	10^{-3}	0.05	$-2(2) \times 10^{-11}$	$-3(2) \times 10^{-12}$	$-8(6) \times 10^{-10}$	-0.14	22.9
2b	_	5×10^{-3}	_	$-1(0.7) \times 10^{-10}$	$-1(0.8) \times 10^{-11}$	$-4(3) \times 10^{-9}$	_	23.1
2c	_	10^{-2}	_	$-2(1) \times 10^{-10}$	$-2(1) \times 10^{-11}$	$-8(6) \times 10^{-9}$	-	23.2
2d	_	5×10^{-2}	_	$-3(2) \times 10^{-10}$	$-3(2) \times 10^{-11}$	$-4(3) \times 10^{-8}$	-	23.5
2e	_	0.1	_	$-3(2) \times 10^{-10}$	$-3(2) \times 10^{-11}$	$-8(7) \times 10^{-8}$	_	23.6
3a	4	10^{-3}	0.1	$-5(4) \times 10^{-11}$	$-2(1) \times 10^{-11}$	$-2(2) \times 10^{-9}$ a	-0.47	32.3
3b	5	_	_	$-4(3) \times 10^{-11}$	$-8(5) \times 10^{-12}$	$-6(5) \times 10^{-10}$ a	-0.24	118.3
3c	6	_	_	$-7(5) \times 10^{-11}$	$-1(0.8) \times 10^{-11}$	$-2(2) \times 10^{-10}$ a	-0.14	274.9
3d	7	_	_	$-2(1) \times 10^{-10}$	$-1(0.8) \times 10^{-11}$	$-8(6) \times 10^{-11}$ a	-0.087	287.8
3e	8	_	_	$-4(3) \times 10^{-9}$	$-9(6) \times 10^{-11}$	$-4(3) \times 10^{-11}$ a	-0.058	21.9
3f	8.25	_	_	$-7(6) \times 10^{-8}$	$-4(3) \times 10^{-10}$	$-3(2) \times 10^{-11}$ a	-0.053	1.1
3g	8.425	_	_	$-7(5) \times 10^{-9}$	$-4(3) \times 10^{-9}$	$-3(2) \times 10^{-11}$ a	-0.050	7.8
3h	9	_	_	$-3(3) \times 10^{-10}$	$-4(3) \times 10^{-11}$	$-2(1) \times 10^{-11}$ a	-0.041	201.0
3i	10	_	_	$-5(4) \times 10^{-11}$	$-4(3) \times 10^{-12}$	$-1(0.7) \times 10^{-11}$ a	-0.030	1235.1
4a	4	10^{-2}	_	$-5(4) \times 10^{-10}$	$-1(0.8) \times 10^{-10}$	$-2(2) \times 10^{-8}$	-0.47	32.4
4b	5	_	_	$-4(3) \times 10^{-10}$	$-7(5) \times 10^{-11}$	$-6(5) \times 10^{-9}$	-0.24	118.7
4c	6	_	_	$-6(5) \times 10^{-10}$	$-9(6) \times 10^{-11}$	$-2(2) \times 10^{-9}$	-0.14	280.4
4d	7	_	_	$-2(1) \times 10^{-9}$	$-1(0.7) \times 10^{-10}$	$-8(6) \times 10^{-10}$	-0.087	315.8
4e	8	_	_	$-7(5) \times 10^{-9}$	$-3(2) \times 10^{-10}$	$-4(3) \times 10^{-10}$	-0.058	110.8
4f	8.25	-	_	$-7(6) \times 10^{-9}$	$-4(3) \times 10^{-10}$	$-3(2) \times 10^{-10}$	-0.053	101.2
4g	8.425	-	_	$-6(5) \times 10^{-9}$	$-4(3) \times 10^{-10}$	$-3(2) \times 10^{-10}$	-0.050	117.1
4h	9	-	_	$-2(2) \times 10^{-9}$	$-2(1) \times 10^{-10}$	$-2(1) \times 10^{-10}$	-0.041	323.9
4i	10	-	-	$-5(3) \times 10^{-10}$	$-3(2) \times 10^{-11}$	$-1(0.7) \times 10^{-10}$	-0.030	1368.7

Note.—Listed are the separation of the system D, the viscous parameter $\alpha_{\rm v}$, the maximum value of H/r, the torque T_z associated with each of the perturbed frequencies 2ω , -2ω and 0, the disk precession frequency ω_p and the ratio of the tidal timescale t_d to the viscous timescale $t_{\nu,\rm h}$.

 $[^]a\mathrm{Cases}$ where, at the outer edge of the disk, g varies on a scale smaller than H.

 $^{^{}b}$ Cases where, at the outer edge of the disk, the radial spherical velocity is larger than the sound speed.

 $^{^{}c}$ Cases where, at the outer edge of the disk, g varies on a scale smaller than H and the radial spherical velocity is larger than the sound speed.

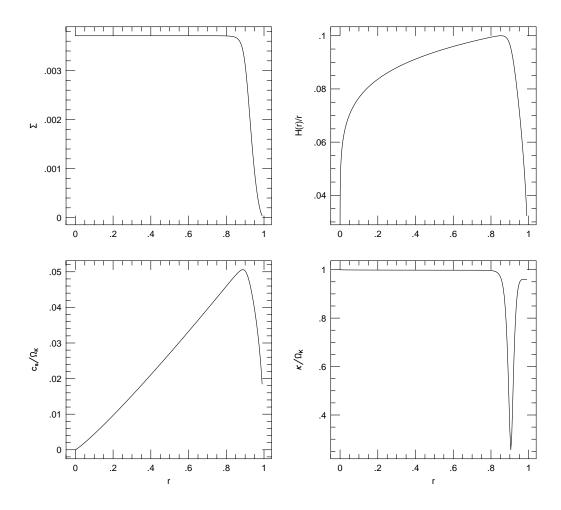
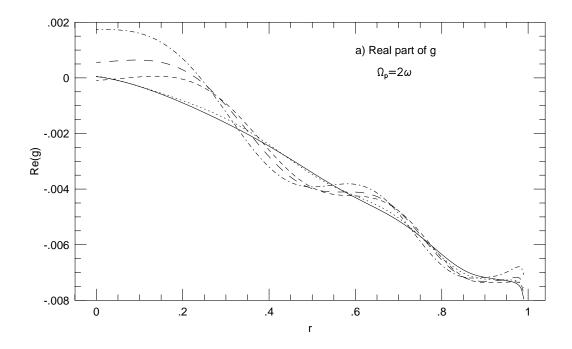


Fig. 1.— Surface mass density (top left), relative semithickness (top right), ratio of the sound speed to the Keplerian frequency (bottom left) and ratio of the epicyclic frequency to the Keplerian frequency (bottom right) vs. r for the equilibrium disk models. The parameters are n=1.5, $M=10^{-2}M_p$ and $(H/r)_{max}=0.1$.



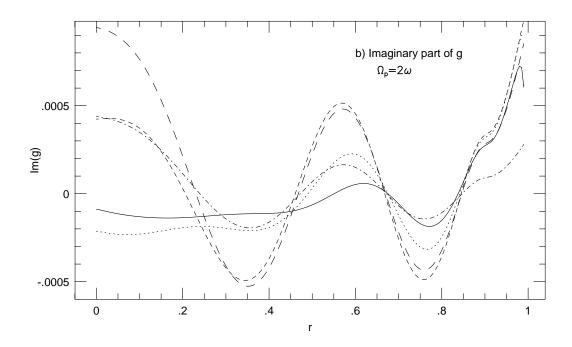
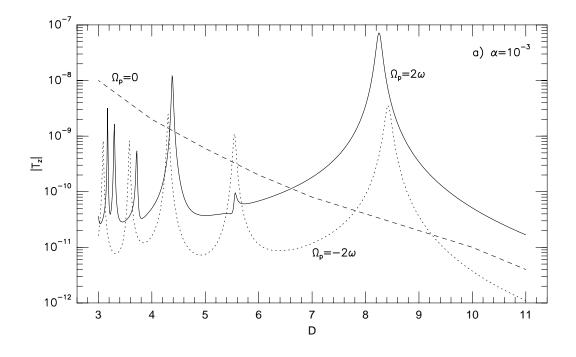


Fig. 2.— Real (panel a) and imaginary (panel b) parts of \tilde{g} vs. r for models 2 and $\Omega_p = 2\omega$. The different curves correspond to $\alpha_{\rm v} = 0.1$ (solid line), 5×10^{-2} (dotted line), 10^{-2} (short dashed line), 5×10^{-3} (long dashed line) and 10^{-3} (dot-short dashed line). The parameters are D=6 and $(H/r)_{max}=0.05$. The wavelike character of the response disappears when $\alpha_{\rm v} \geq H/r$.



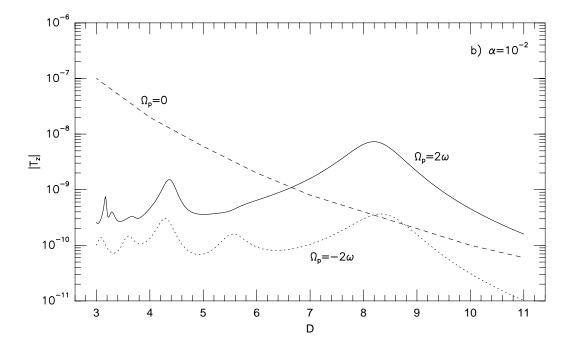
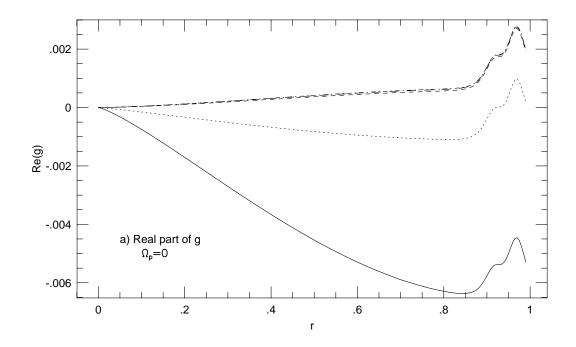


Fig. 3.— Net torque $|T_z|$ vs. D in a semilog representation for $(H/r)_{max}=0.1$. The panels a and b correspond to $\alpha_{\rm v}=10^{-3}$ (models 1b and 3) and $\alpha_{\rm v}=10^{-2}$ (models 1c and 4) respectively. The different curves correspond to $\Omega_p=2\omega$ (solid line), -2ω (dotted line) and 0 (dashed line). These plots show several resonances.



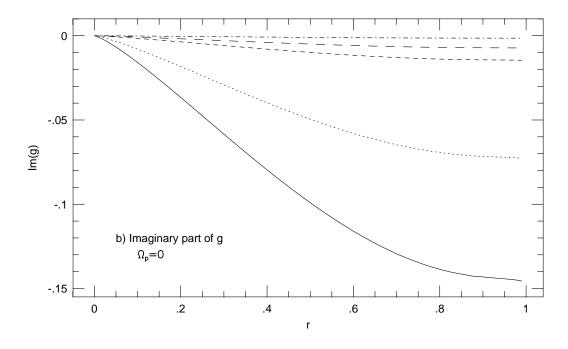


Fig. 4.— Real (panel a) and imaginary (panel b) parts of \tilde{g} vs. r for models 2 and $\Omega_p=0$. The different curves correspond to $\alpha_{\rm v}=0.1$ (solid line), 5×10^{-2} (dotted line), 10^{-2} (short dashed line), 5×10^{-3} (long dashed line) and 10^{-3} (dot-short dashed line). The parameters are D=6 and $(H/r)_{max}=0.05$. The zero–frequency response is not wave–like.

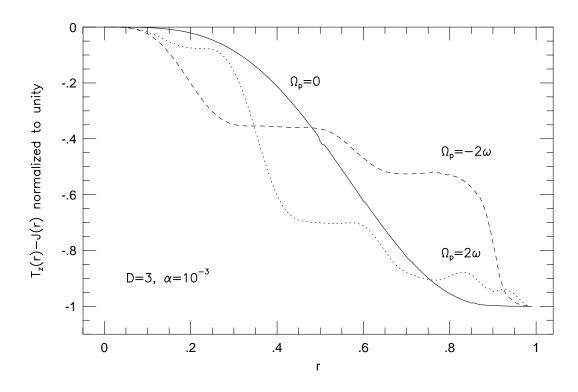


Fig. 5.— $T_z(r)-J(r)$ (angular momentum dissipated between r_{in} and r) normalized to unity vs. r for $\alpha=10^{-3},\,D=3$ (model 1b) and $\Omega_p=0$ (solid line), 2ω (dotted line) and -2ω (dashed line).

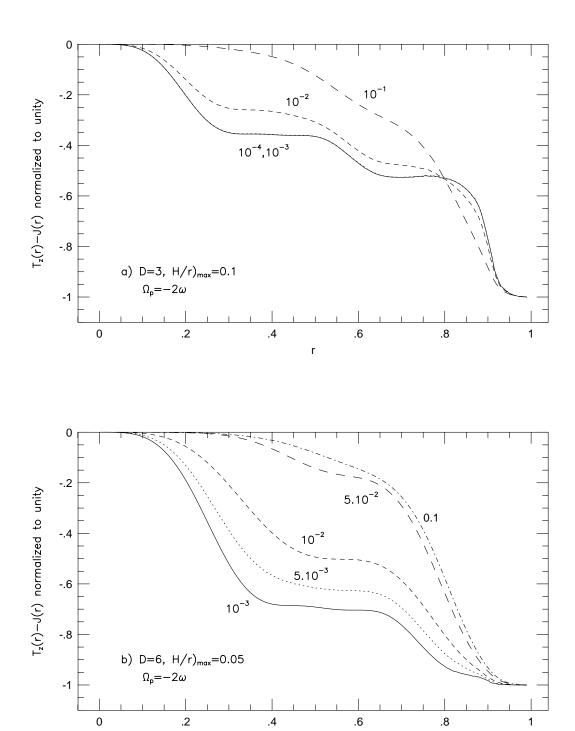
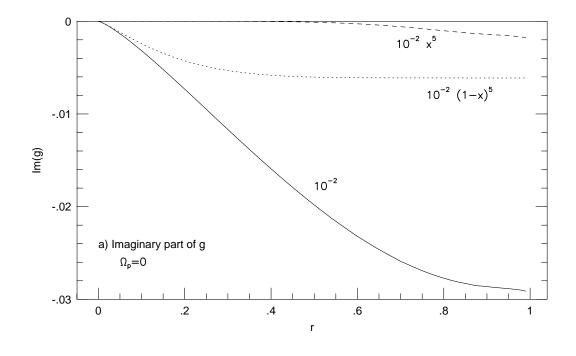


Fig. 6.— $T_z(r)-J(r)$ (angular momentum dissipated between r_{in} and r) normalized to unity vs. r for $\Omega_p=-2\omega$. The panel (a) corresponds to models 1, i.e. D=3, $(H/r)_{max}=0.1$ and $\alpha=10^{-4}$ (solid line), 10^{-3} (dotted line), 10^{-2} (short dashed line) and 0.1 (long dashed line). The panel (b) corresponds to models 2, i.e. D=6, $(H/r)_{max}=0.05$ and $\alpha=10^{-3}$ (solid line), 5×10^{-3} (dotted line), 10^{-2} (short dashed line), 10^{-2} (long dashed line) and 0.1 (dot-short dashed line).



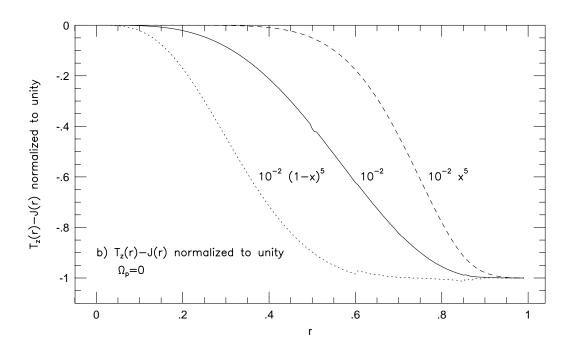


Fig. 7.— Imaginary part of \tilde{g} (panel a) and $T_z(r) - J(r)$ (angular momentum dissipated between r_{in} and r) normalized to unity (panel b) vs. r for $\Omega_p = 0$ and a nonuniform α . The different curves correspond to $\alpha = 10^{-2}$ (solid line), $10^{-2} (1-x)^5$ (dotted line) and $10^{-2} x^5$ (dashed line). The parameters are D=3 and $(H/r)_{max}=0.1$.